iScience

CellPress
OPEN ACCESS

Article

Differential immunometabolic responses to Delta and Omicron SARS-CoV-2 variants in golden syrian hamsters

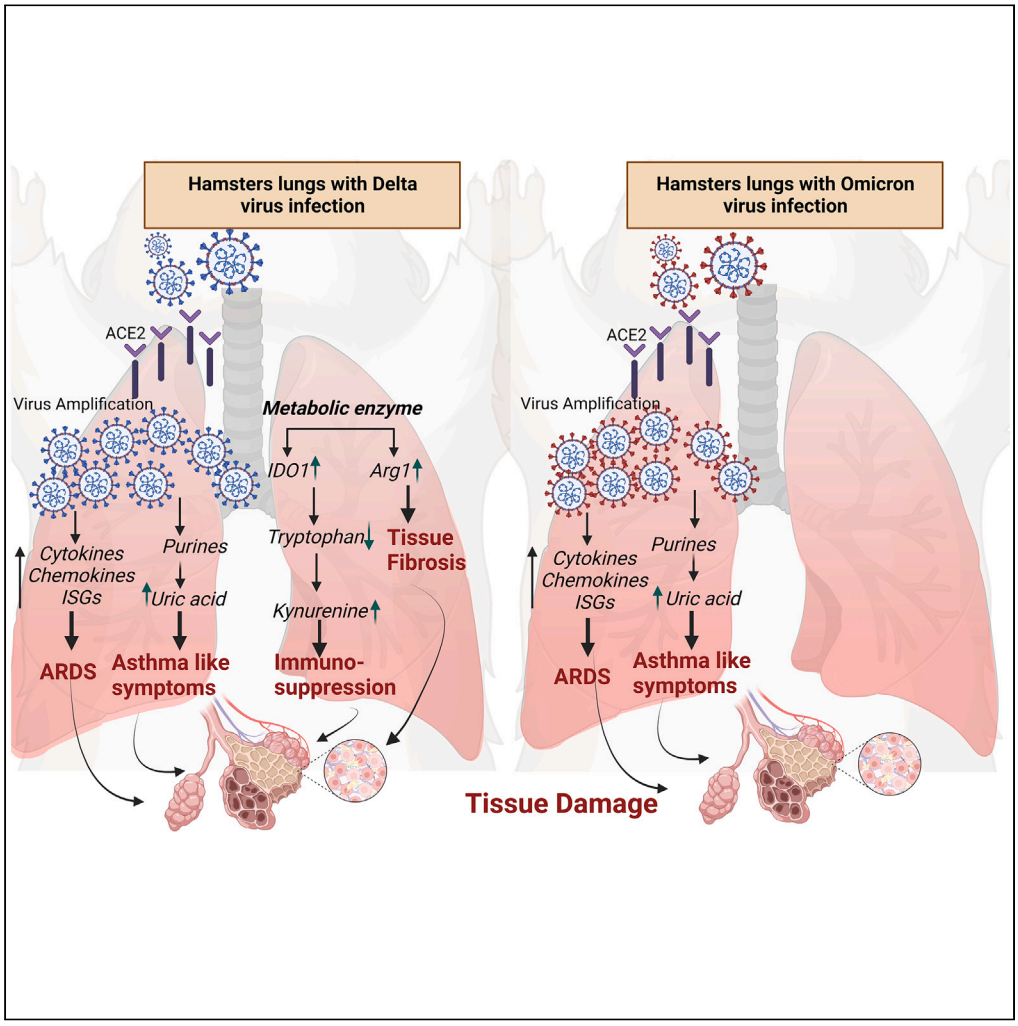

Rajesh Rajaiah, Kabita Pandey, Arpan Acharya, ..., Samuel M. Cohen, Ujjwal Neogi, Siddappa N. Byrareddy

sid.byrareddy@unmc.edu

Highlights

SARS-CoV-2 Delta variant augmented lung pathology in golden syrian hamsters

Delta variant increased the expression of immune mediators and metabolic enzymes

Delta and Omicron variants imparted differential regulation of metabolism in lungs

Rajaiah et al., iScience 27, 110501
August 16, 2024
https://doi.org/10.1016/j.isci.2024.110501

iScience

CellPress
OPEN ACCESS

Article

Differential immunometabolic responses to Delta and Omicron SARS-CoV-2 variants in golden syrian hamsters

Rajesh Rajaiah,[1] Kabita Pandey,[1] Arpan Acharya,[1] Anoop Ambikan,[3] Narendra Kumar,[1,8] Reema Guda,[1] Sean N. Avedissian,[4] Luis J. Montaner,[5] Samuel M. Cohen,[2] Ujjwal Neogi,[3] and Siddappa N. Byrareddy[1,2,6,7,9,*]

SUMMARY

Delta (B.1.617.2) and Omicron (B.1.1.529) variants of SARS-CoV-2 represents unique clinical characteristics. However, their role in altering immunometabolic regulations during acute infection remains convoluted. Here, we evaluated the differential immunopathogenesis of Delta vs. Omicron variants in Golden Syrian hamsters (GSH). The Delta variant resulted in higher virus titers in throat swabs and the lungs and exhibited higher lung damage with immune cell infiltration than the Omicron variant. The gene expression levels of immune mediators and metabolic enzymes, Arg-1 and IDO1 in the Delta-infected lungs were significantly higher compared to Omicron. Further, Delta/Omicron infection perturbed carbohydrates, amino acids, nucleotides, and TCA cycle metabolites and was differentially regulated compared to uninfected lungs. Collectively, our data provide a novel insight into immunometabolic/pathogenic outcomes for Delta vs. Omicron infection in the GSH displaying concordance with COVID-19 patients associated with inflammation and tissue injury during acute infection that offered possible new targets to develop potential therapeutics.

INTRODUCTION

Severe acute respiratory syndrome coronavirus-2 (SARS-CoV-2) is an enveloped, positive-sense, single-stranded RNA virus and a causative agent of COVID-19.[1–3] SARS-CoV-2 mainly infects host cells via angiotensin-converting enzyme 2 (ACE-2) receptor, which is highly expressed on various epithelial cells in target organs, including the lungs, intestine, and heart, among other organs.[4,5] Since 2020, the emergence of SARS-CoV-2 variants of concern (VOCs) bearing multiple mutations, which is responsible for higher infection rates and mortality.[6] Among the VOCs, Delta (B.1.617 lineage) is more pathogenic, which has caused a higher risk of hospitalization with severe respiratory illness and increased mortality among COVID-19 patients.[7] The Delta variant showed global dominance from December 2020 to October 2021, now surpassed by the Omicron variant.[8,9] Before recovering from the severe crisis caused by the Delta variant, the emergence of the Omicron variant exacerbated the pandemic situation.[10] Omicron variants BA.1, BA.2, BA.3, BA.4, and BA.5 are responsible for the recent infection surge globally.[10–12] Even though various vaccines have helped reduce mortality and hospitalization, they cannot control the transmission and emergence of new variants.[13]

Host immune response plays a crucial role in combating SARS-CoV-2 infection. However, the hyperactivation or dysregulation of immune response is detrimental to the host that has been reported upon SARS-CoV-2 infection.[14–17] It is well established that metabolic pathways tightly regulate the immune responses, and SARS-CoV-2 is known to hijack the host immunometabolic pathways to evade the host immune response.[15,18–20] An anti-inflammatory cytokine IL-10, and amino acid metabolic enzymes, including arginase 1 (Arg1) and indoleamine 2,3-dioxygenase 1 (IDO1), have been implicated in SARS-CoV-2-induced pathology in COVID-19 patients.[21–23] IL-10, Arg1, and IDO1 are immunosuppressive and known to mitigate host immune responses that may support SARS-CoV-2 replication in the host. Further, the involvement of IL-10 and Arg1 has been well established in viral infection and tissue fibrosis.[24–26] Moreover, metabolites derived from tryptophan, adenosine, and collagen catabolism have been associated with SARS-CoV-2-induced lung damage.[22,27,28] Hence, it is important to understand the role of host metabolic flux and the dysregulated immune response to correlate Delta variants-induced severe pathology compared to

[1]Department of Pharmacology and Experimental Neuroscience, University of Nebraska Medical Center, Omaha, NE, USA
[2]Havlik Wall Professor of Oncology, Department of Pathology and Microbiology, University of Nebraska Medical Center, Omaha, NE, USA
[3]The Systems Virology Lab, Department of Laboratory Medicine, Division of Clinical Microbiology, ANA Futura, Karolinska Institutet, 141 52 Stockholm, Sweden
[4]Antiviral Pharmacology Laboratory, College of Pharmacy, University of Nebraska Medical Center, Omaha, NE, USA
[5]Vaccine and Immunotherapy Center, The Wistar Institute, Philadelphia, PA 19104, USA
[6]Department of Genetics, Cell Biology and Anatomy, University of Nebraska Medical Center, Omaha, NE, USA
[7]Department of Biochemistry and Molecular Biology, University of Nebraska Medical Center, Omaha, NE, USA
[8]Present address: Department of Biochemistry, Daulat Ram College, University of Delhi, Delhi, India
[9]Lead contact
*Correspondence: sid.byrareddy@unmc.edu
https://doi.org/10.1016/j.isci.2024.110501

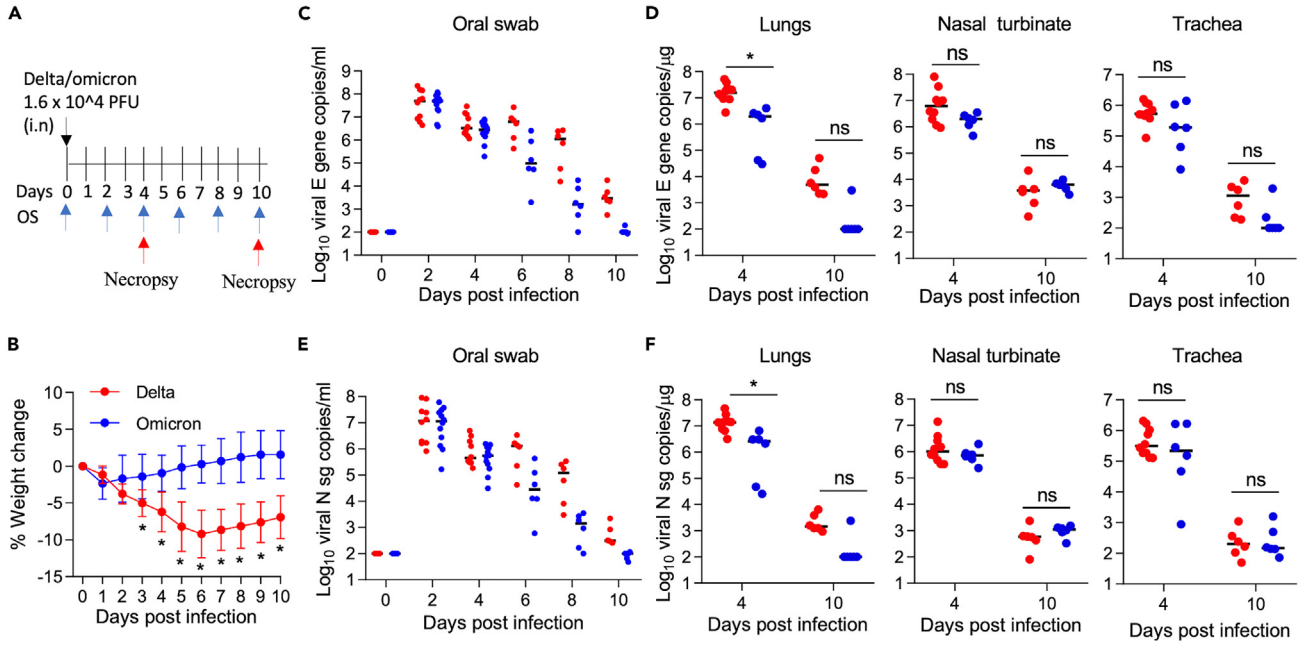

Figure 1. Productive infection of SARS-CoV-2 variants in golden Syrian hamsters (GSH)

Golden Syrian hamsters were intranasally infected with Delta and Omicron variants (1.6 x 104 PFU/animal). Weights were recorded daily, and oral swabs were collected every alternative day, as indicated in blue arrows. Hamsters were euthanized on 4 and 10 DPI, as shown in red arrows (A). Body weight loss was calculated as percent weight change (B). Lungs, nasal turbinate, and trachea were collected on 4 and 10 DPI, and RNA was isolated. SARS-CoV-2 E gene genomic RNA (C and D) and N gene subgenomic RNA (E and F) were quantitated in oral swabs and tissues by RT-qPCR using specific primers and probes. Data represent the mean ± SEM. *$p < 0.05$, Delta vs. Omicron treated groups. ns, non-significant.

Omicron variants. Golden Syrian hamsters (GSH) and ACE-2 transgenic mouse models have been extensively explored for viral replication competence, transmission, host immune response, preclinical drug/vaccine screening, and establishing new therapeutic targets for coronaviruses, including SARS-CoV-1, MERS-CoV, and SARS-CoV-2.[4,8,29–31] Although the Omicron variants are shown to be less pathogenic in humans, they infect GSH and transgenic mice like the Delta variant with limited pathogenicity in respiratory organs.[11,32]

The primary clinical manifestation in COVID-19 patients is severe lung inflammation.[5,33] SARS-CoV-2 induces a hyperactive immune response in the target organ and systemic inflammation, leading to acute respiratory distress syndrome (ARDS).[34–36] SARS-CoV-2 variants, including Delta and Omicron, possess spike protein mutations and are known for increased transmissibility and variable pathogenicity.[37–39] GSH becomes infected naturally with SARS-CoV-2 and shows disease pathology like COVID-19 patients.[40,41] The GSH model is a suitable preclinical model for studying vaccine efficacy, immunopathogenesis, virus replication kinetics, transmissibility, and finding novel therapeutic targets and therapeutic molecules to prevent/treat SARS-CoV-2-induced pathology.[29,30,42] Several reports demonstrated the pathogenicity, replication kinetics, and host immune response against SARS-CoV-2 in GSH.[3,8,11,29,30,43] Further, the GSH model is also being used to understand the mechanism of development of post-acute sequelae of COVID-19 (PASC), including neuro-PASC.[44,45] However, the differential immunometabolism and immunopathogenesis of Delta and Omicron variants *in vivo* and *in vitro* have not been well established. Therefore, we have evaluated Delta and Omicron variants-mediated immunopathogenesis and immunometabolism in GSH and Calu-3 cells. We found the differential immune regulation between the variants with possible involvement of metabolic enzymes (Arg1 and IDO1), and hypoxic conditions by upregulation of metabolites, including aconitic acid, 2-hydroxyglutaric acid, and uric acid. Overall, the present study pronounced the immunoregulation mechanisms induced by the Delta variant that support its significantly elevated pathogenic role over Omicron.

RESULTS

SARS-CoV-2 delta and omicron variants exhibited differential replication kinetics in GSH

GSH is a widely studied and accepted preclinical model to study the immunopathogenesis of coronaviruses, including SARS-CoV-1, MERS-CoV, and SARS-CoV-2 and its variants.[8,29,31] Given that the SARS-CoV-2 Delta variant is more pathogenic than the Omicron variant in humans, we compared their replication kinetics in the GSH model. GSH were inoculated intranasally with $1.6x10^4$ of plaque forming unit (PFU)/animal of Delta (hCoV-19/USA/PHC658/2021; $n = 12$, six sacrificed at 4 days post-infection (DPI) and six sacrificed 10 DPI) or Omicron (hCoV-19/USA/GA-EHC-2811C/2021; $n = 12$, six sacrificed at 4 DPI and six sacrificed 10 DPI) variants (Figure 1A). First, hamsters were observed for change in body weight daily. Upon infection with the Delta, hamsters started losing body weight from 1 DPI with maximum weight loss at 6 DPI, and the

body weight did not return to the baseline even at 10 DPI (Figure 1B). In contrast, hamsters infected with Omicron did not lose body weight (Figure 1B).

Next, we quantified the SARS-CoV-2 viral RNA by RT-qPCR in the oral swabs collected every alternative day till 10 DPI. For both the E gene and N sub gene (sg), the viral RNA copies were comparable without a significant difference in oral swabs from hamsters infected with Delta and Omicron variants with peak viral load detected at 2 DPI (Figures 1C and 1D). We quantitated the viral RNA level in the lungs and other respiratory-associated tissues, such as trachea and nasal turbinates, in Omicron vs. Delta-infected hamsters at 4 and 10 DPI (Figures 1E and 1F). At 4 DPI, we observed a significantly higher level of viral RNA (for both the E gene and N sg) between Delta vs. Omicron-infected GSH. Further, immunohistochemistry of hamster lungs showed the presence of SARS-CoV-2 spike (Figure S1A) and nucleocapsid (Figure S1B) proteins in Delta and Omicron-infected animals at 4 DPI. On 10 DPI, viral spike and nucleocapsid protein expression were not sustained in virus infected GSH lungs (Figures S1A and S1B). We also examined the possibility of neurotropism of SARS-CoV-2 variants by testing the presence of viral RNA copies in GSH brain tissues. Although we have found a relatively low viral RNA load at 4 DPI in the brain infected with the Delta variant (Figure S2A), the histopathological (Figure S2B) and immunohistochemical (Figures S2C and S2D) results did not support the presence of viral RNA in the brain at 10 DPI. We performed a correlation analysis using the Pearson correlation coefficient between the longitudinal viral loads in oral swabs (2, 4, 6, 8, and 10 DPI) with respiratory tract tissue (4 and 10 DPI) viral loads to understand the relation between the viral shedding with tissue reservoirs. A strong positive correlation was observed in the SARS-CoV-2 E gene and N sg concentration between 2 DPI oral swabs and lung tissues at 4 DPI for Delta and Omicron infected GSH (Figures S3A–S3D; Tables S1A–S1D).

The SARS-CoV-2 delta variant induced augmented lung damage compared to the omicron variant in GSH

The histopathological examination of the lungs of hamsters infected with the Delta variant revealed severe congestion, bronchial/bronchiolar hyperplasia, immune cell infiltration, edema, and inflammation at 4 DPI. In contrast, the Omicron variant did not affect the lung architecture (Figure 2A). Interestingly, the lung tissues from hamsters infected with the Delta variant compared to the Omicron variant exhibited increased collagen fibers established by the intensity of Picro Sirius red staining (Figure 2B). The Picro Sirius red staining persisted at 10 DPI in the Delta-infected lung compared to Omicron-infected lungs (Figure 2B). The presence of collagen fibers in the lungs is an indicator of tissue fibrosis. These data suggested that lung tissue damage/fibrosis persists in Delta infected hamsters even after recovery from peak viral infection.

Delta and omicron variants induced differential gene expression of cytokines, chemokines, and ISGs

The host immune response to the SARS-CoV-2 virus is hyperinflammatory, releasing many pro-inflammatory cytokines that initiate inflammation-induced lung injury associated with pneumonitis and ARDSs.[46–48] The measurement of cytokine secretion in the hamster is limited; hence, we used RT-qPCR to analyze the gene expression profile of cytokines, chemokines, interferon stimulatory genes (ISGs), and metabolic enzymes, including Arg1 and IDO1 in the lungs. We found that the gene expression of proinflammatory cytokine IL-6 was upregulated in hamster lungs infected with Delta variant at 4 DPI compared to Omicron-infected hamster lungs (Figure 3A). Another proinflammatory cytokine, TNF-α gene expression, was upregulated over naive without a marked difference between Delta and Omicron-infected lungs (Figure 3A). In contrast, IL-10 is an anti-inflammatory cytokine highly upregulated at 4 DPI in Delta-infected hamster lungs compared to Omicron. Further, the Th1 cytokine IFN-γ, but not Th2 cytokine IL-4 gene expression was elevated at 4 DPI compared to 10 DPI in Delta vs. Omicron-infected lungs (Figure 3A). Distinct from the lungs, the expression of the cytokines in the brain was not elevated at 4/10 DPI during either Delta or Omicron infection (Figure S4A).

ISGs and chemokines are critical in the host antiviral response.[49] ISG15 is a ubiquitin-like protein induced by type I interferons, whereas CXCL10, is a chemokine induced by both type I and II interferons.[49,50] The gene expression of ISG15 was increased in Delta- and Omicron-infected lungs over the naive at 4 DPI (Figure 3B), which started to be diminished by 10 DPI. CCL5 is a chemoattractant for various immune cells, including monocytes, memory Th cells, and eosinophils, and its expression is induced by IFN-γ and TNF-α.[51] The gene expression of CCL5 in Delta and Omicron-infected lungs was induced over naive at 4 DPI (Figure 3B). Interestingly, the gene expression of CCL5 in Delta-infected lungs was sustained even at 10 DPI, on the contrary, in the Omicron-infected lungs, that was reduced to the baseline by 10 DPI (Figure 3B). Moreover, the gene expression of ISG15 and CCL5 was also elevated in the brain of hamsters infected with either Delta or Omicron (Figure S4B).

Delta and omicron variants distinctly regulated the gene/protein expression of metabolic enzymes Arg1 and IDO1 in the lungs

Amino acid-depleting enzymes, including arginase-1 (Arg1), inducible nitric oxide synthase (iNOS), and IDO play a critical role in host immune response.[52–55] Therefore, we evaluated the gene expression profile of these metabolic enzymes in the Delta and Omicron-infected lung tissues. The gene expression of Arg1 and IDO1 was increased in the lungs infected with Delta at 4 DPI, which returned to the baseline levels by 10 DPI (Figure 3C). In contrast, the gene expression of iNOS remained unaltered in the lung tissues infected with either Delta or Omicron (Figure 3C). Interestingly, the gene expression of Arg1 was upregulated over naive in brain tissues from hamsters infected with either Delta or Omicron variant at 10 DPI (Figure S4C).

Further, we confirmed by immunoblotting that at 4 DPI the protein level of Arg1 was elevated in Delta infected lungs compared to the uninfected and Omicron infected lungs (Figures 3D and 3E), which correlates with the gene expression of Arg1 (Figure 3C). However,

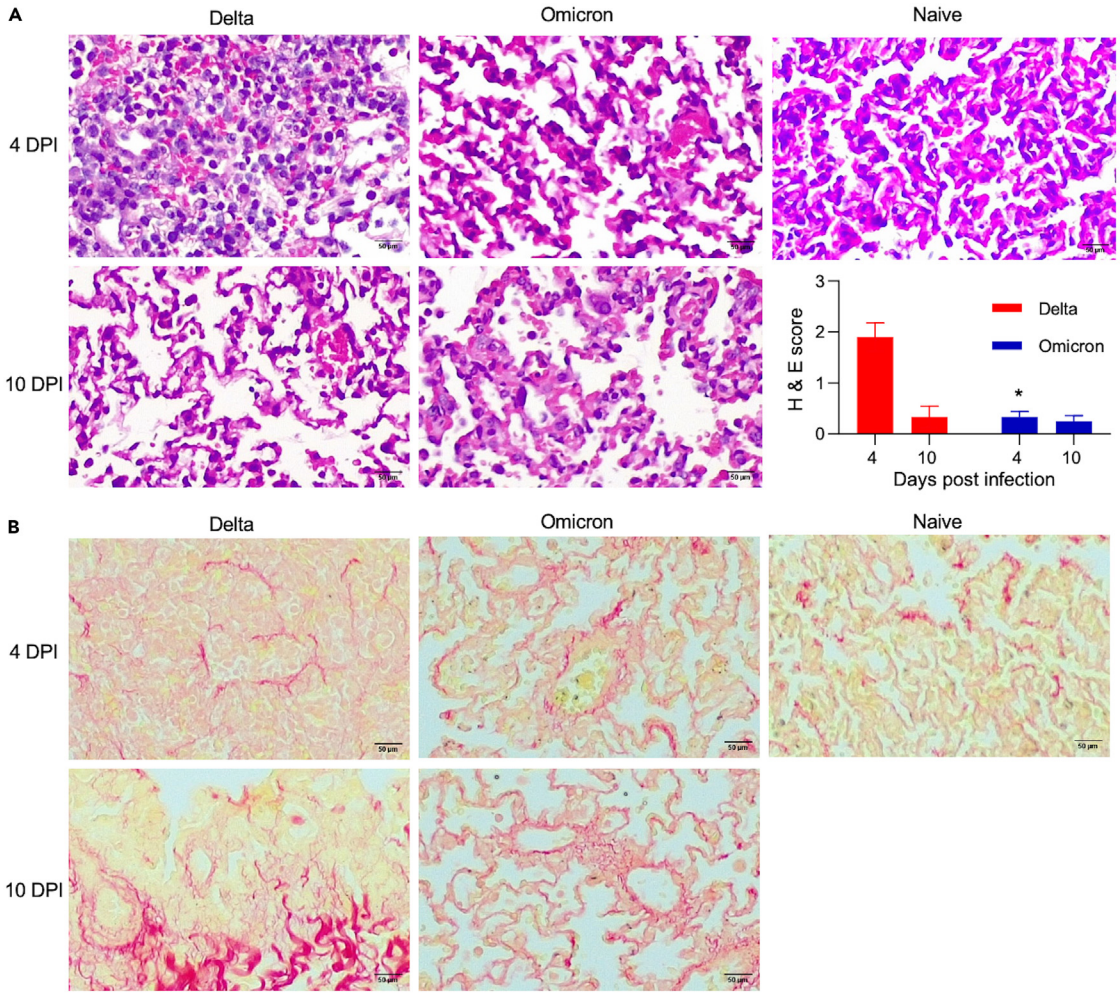

Figure 2. Hematoxylin & eosin, and picrosirius red staining of lung tissue sections from hamsters infected with SARS-CoV-2 variants

Lung tissues on 4 and 10 DPI were fixed in 10% neutral buffered formalin and processed. (A) Five-micron tissues were stained with H & E and slides were analyzed for histopathological scoring, and images were captured under the light microscope at 20X. (B) Tissue sections were stained with picrosirius red staining for collagen, and images were captured at 20X under a light microscope. Magnification 200×. Scale bars, 50 μm. Data represent the mean ± SEM. *$p < 0.05$, Delta vs. Omicron treated groups.

the gene expression of IDO1 (Figure 3C) was not associated with increased protein expression in SARS-CoV-2-infected lungs (Figure 3D). This could be due to the specificity of IDO antibody toward human IDO, which may not be cross-reactive with hamster IDO. In these experiments, mouse liver and IFN-γ stimulated Calu-3 cell lysates were used as a positive control for the Arg1 and IDO-specific antibodies, respectively.

Delta and omicron infection perturbed carbohydrates, amino acids, pyrimidine, purine, and tricarboxylic acid metabolites in GSH lung tissues

Immune cells utilize substantial metabolic resources during infection and inflammation.[56–58] Pathogens can modulate the host immunometabolism to adapt to host target tissues, which assists in extended infection and transmission.[56] We evaluated the targeted metabolomics profile in Delta- and Omicron-infected lungs at 4 DPI compared to uninfected lung tissues. The principal-component analysis (PCA) plot indicates the clear separation between Delta- and Omicron-infected lung tissues with 25% and 22% variances on PC1 and PC2, respectively (Figure 4A). Several metabolites, including kynurenine, dihydrouracil, uric acid, and thymine, were upregulated, and methyladenine, sedoheptulose, niacin, and carnitine were downregulated in Delta-infected lung tissues compared to naive (Figure 4B). Similarly, metabolites dihydrouracil, uric acid, and NADPH were upregulated, and methyladenine, niacin, and urocanic acid were downregulated in Omicron-infected lung tissues compared to naive (Figure 4C). The differential perturbation in metabolites between Delta- and Omicron-infected lung tissues is

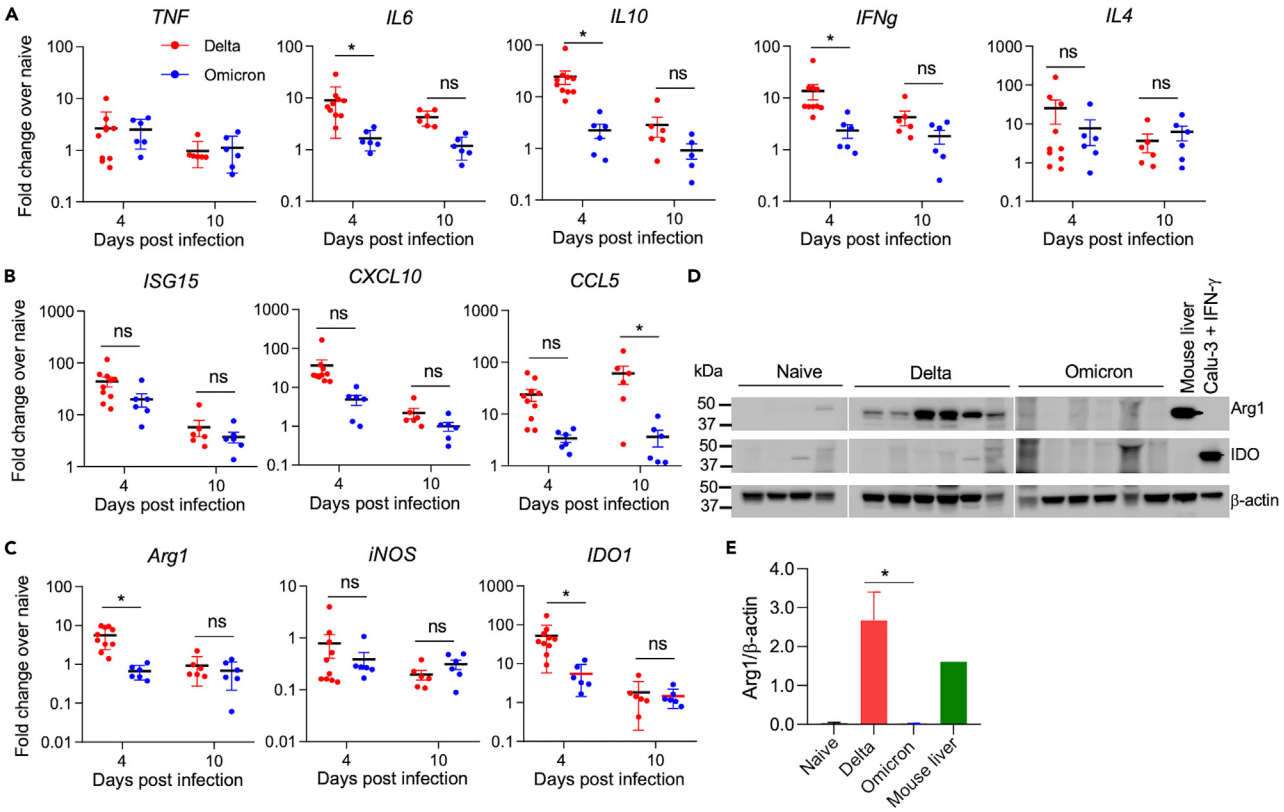

Figure 3. Gene expression profiles of cytokines, ISGs/chemokines, and metabolic enzymes, and protein expression of metabolic enzymes in hamster lung tissues infected with SARS-CoV-2 variants RNA was isolated from lung tissues after 4 and 10 DPI, and cDNA was synthesized

Gene expression profiles of cytokines (A), ISGs/chemokines (B), and metabolic enzymes (C) were analyzed by RT-qPCR using golden Syrian hamster gene-specific primers. Western blotting analyzed whole lung tissue lysates from hamsters for protein expression of Arg1 and IDO (D and E). Mouse liver lysate was used as a positive control for Arg1, and IFN-g-treated Calu-3 cell lysate was used as a positive control for IDO. Data represent the mean ± SEM. *$p < 0.05$, Delta vs. Omicron treated groups. ns, non-significant.

shown in Figure 4D. The heatmap shows increased and decreased carbohydrates, amino acids, pyrimidine, purine, and tricarboxylic acid (TCA) cycle metabolites in infected lung tissues (Figure 4E). Remarkably, tryptophan and its metabolite, kynurenine, were reciprocally regulated in lung tissues infected with the Delta variant (Figure 4E). The ratio of kynurenine and tryptophan was higher in lung tissues infected with the Delta variant (Figure 4E), indicating the increased enzymatic activity of IDO. Additionally, tryptophan is an essential amino acid required for T cell response, and its metabolite, kynurenine, has been associated with immune suppression.[59,60] Collagen is an integral component of the extracellular matrix of amino acids proline/hydroxyproline, alanine, and glycine.[61] Hydroxyproline and alanine, originating from collagen metabolism,[28] were reduced in lungs infected with the Delta variant but not in Omicron-infected lungs (Figure 4F). It is well known that SARS-CoV-2 infection induces hypoxia, which causes the elevation of metabolites aconitic acid, 2-hydroxyglutaric acid, and uric acid.[62] In the Delta-infected lungs, the hypoxia-mediated metabolites, 2-hydroxyglutaric acid, and uric acid were elevated at 4 DPI (Figure 4F).

On the other hand, aconitic acid, an intermediate of the TCA cycle, was reduced in lung tissue infected with Delta and Omicron (Figure 4F). Niacin, a metabolite of tryptophan and nicotinamide, the precursors of NAD^+ and $NADP^+$, was decreased in lung tissues infected with Delta and Omicron variants (Figure 4F). NADPH is an essential antioxidant in neutralizing reactive oxygen species generated during oxidative stress induced by external stimuli, including infection.[63] Unlike niacin and nicotinamide, NADPH levels increased in lung tissues infected with Delta and Omicron variants (Figure 4F).

SARS-CoV-2 variants induced differential gene expression of cytokines, chemokines, ISGs, IDO1, and protein expression of IDO in Calu-3 cells

To understand the differential immunopathogenesis of Delta vs. Omicron, we investigated the comparative replication kinetics of Delta, Omicron, and the ancestral strain of SARS-CoV-2 in Calu-3 cells. All three variants exhibited replication competence and infectivity in Calu-3 cells, which were confirmed by the amplification of the E gene and N sub-gene by RT-qPCR (Figure S5). Further, we evaluated the differential regulation of host gene expression by these three strains of SARS-CoV-2. All three variants induced differential gene expression of cytokines,

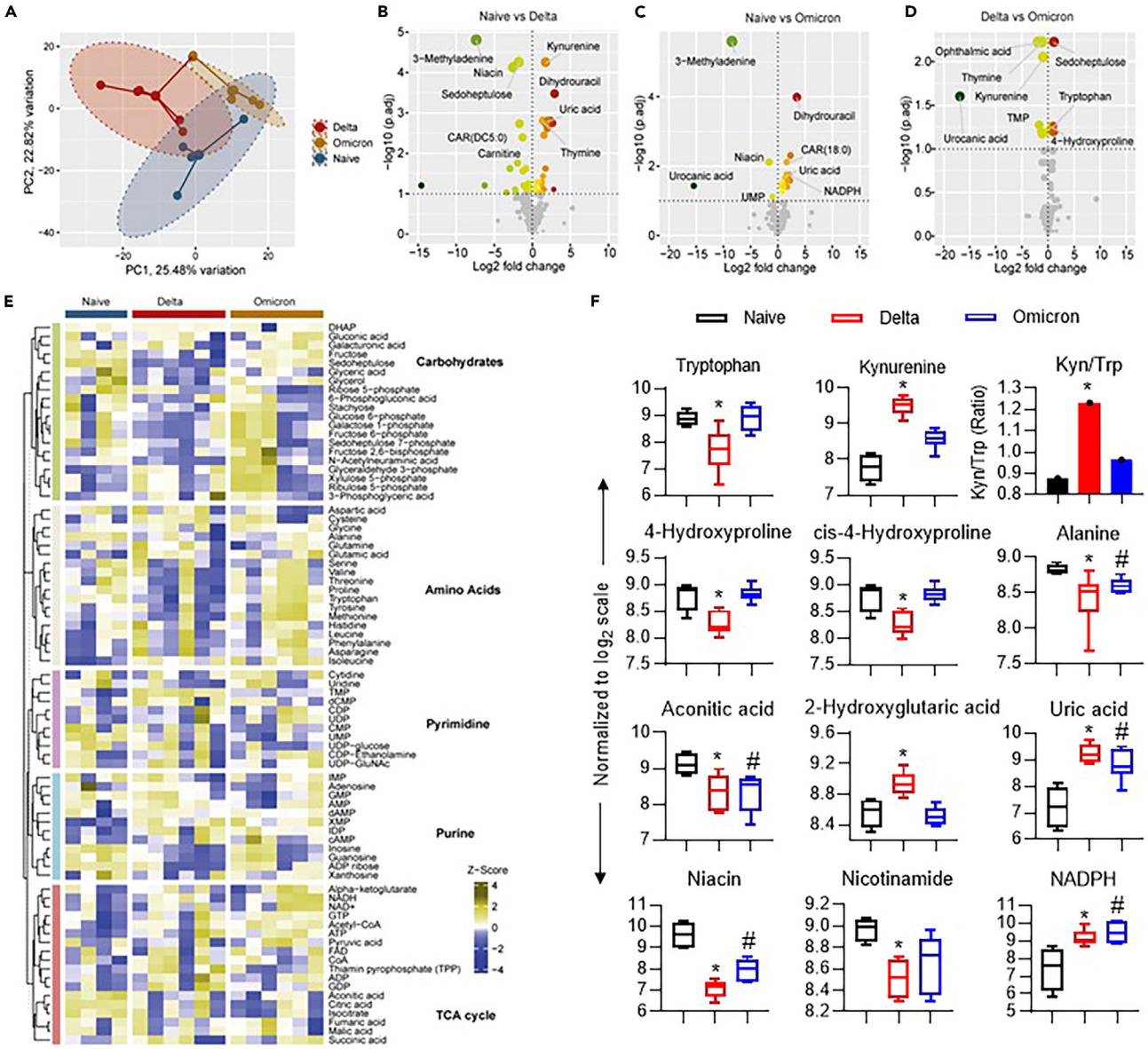

Figure 4. Metabolomic profiles for carbohydrates, amino acids, pyrimidine, purine, and TCA cycle metabolites in lung tissues from hamsters infected with SARS-CoV-2 variants

SARS-CoV-2 infected hamster lung tissues were analyzed for untargeted metabolites by LC-MS. Samples distribution was analyzed by PCA plots of metabolome changes in lung tissues infected with SARS-CoV-2 variants compared to uninfected Naive lung tissue (A). Volcano plots of dysregulated metabolites in Naive vs. Delta (B), Naive vs. Omicron (C), and Delta vs. Omicron (D) in hamster lung tissues. The *p*.adj values are computed using limma and multiple hypotheis test correction was performed using Benjamini-Hochberg method. Heatmap showing the perturbation of carbohydrates, amino acids, pyrimidine, purine, and TCA cycle components in the lung tissues of uninfected and SARS-CoV-2-infected hamsters (E). Significantly altered metabolites in SARS-CoV-2 infected hamster lung tissues were compared to Naive lung tissues (F). Data represent the mean ± SEM. **p* < 0.05, naive vs. Delta; #*p* < 0.05, naive vs. Omicron treated groups.

chemokines, ISGs, and metabolic enzyme IDO1 that peaks at 48 h post-infection time (Figure 5A). The Delta variant increased cytokine, chemokine, ISGs, and IDO1 gene expression (Figures 5A and 5B). The gene expression of IDO1 was correlated to its protein expression mediated by all three variants (Figures 5C and 5D). Unlike hamster lung tissues (Figures 3C and 3D), Arg1 gene and protein expression were not detected in Calu-3 cells upon infection with SARS-CoV-2 variants. We reasoned that inhibition of IDO may reduce SARS-CoV-2 replication in Calu-3 cells. However, a competitive inhibitor (indoximod or 1-methyl tryptophan) of IDO failed to inhibit Delta virus replication in Calu-3 cells even at 0.1 MOI (Figure S6).

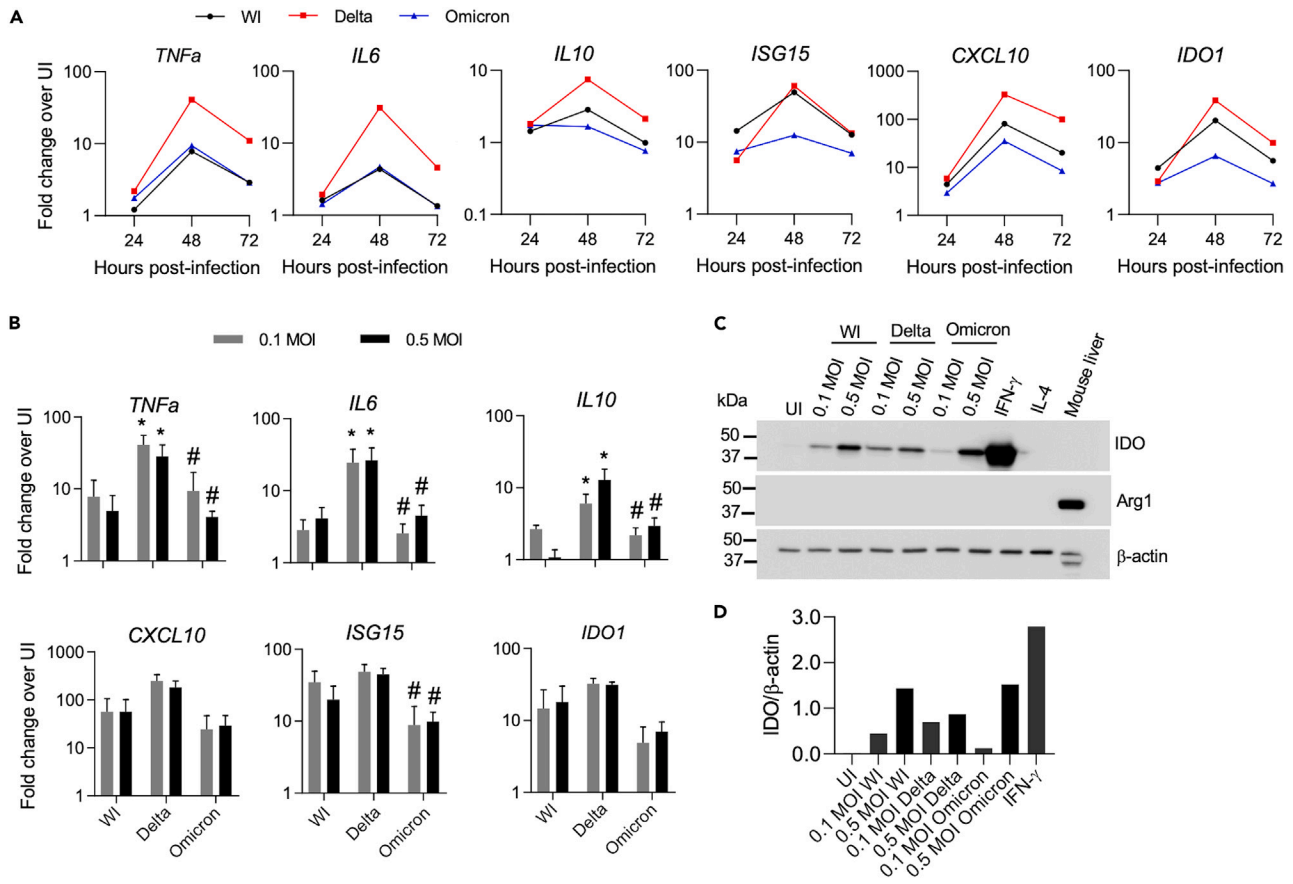

Figure 5. Gene expression profiles of cytokines, ISGs/chemokines and metabolic enzymes, and protein expression of IDO in Calu-3 cells infected with SARS-CoV-2 variants

Calu-3 cells (2 x 105) were infected with SARS-CoV-2 variants with 0.1 MOI for 24–72 h (A) and with different MOI of 0.1 and 0.5 for 48 h (B). RNA was isolated, cDNA was synthesized, and gene expression profiles were analyzed by RT-qPCR using human gene-specific primers (A and B). Whole-cell lysates from SARS-CoV-2-infected Calu-3 cells (1 x 106) were analyzed for protein expression of IDO by western blotting (C and D). Data represent the mean ± SEM. *$p < 0.05$, WI vs. Delta; #$p < 0.05$, Delta vs. Omicron treated groups.

IL-10 did not potentiate delta variant replication and failed to inhibit virus-induced host gene expression

In COVID-19 patients, the plasma levels of IL-6 and IL-10 are correlated with disease severity.[64] IL-10 is a pleiotropic cytokine with immunosuppressive as well as immuno-stimulatory activities. To verify the effect of IL-10 on replicative kinetics and differential host gene expression by Delta variant, we infected Calu-3 cells with Delta in the absence or presence of recombinant human IL-10. We quantitated the viral E gene in cellular and culture supernatant. Although IL-10 has been linked to disease severity in COVID-19 patients, it did not potentiate the replication of the Delta variant at 0.01 MOI (Figure 6A). Instead, IL-10 reduced viral RNA copies in the culture supernatant of Calu-3 cells infected with the Delta variant (Figure 6A). On the other hand, IFN-γ, an anti-viral cytokine, reduced the replication of the Delta variant in cellular and culture supernatant (Figure 6B). Further, IL-10 failed to reduce virus-induced host gene expression at 5 and 10 ng/mL in contrast to IFN-γ effects in decreasing TNF-α at 10 and 20 ng/mL concentrations (Figure 6D). Of interest, the gene expression of virus-induced IL-6, ISG15, CXCL10, and IDO1 was not affected by IFN-γ (Figure 6D), although IFN-γ alone (10 ng/mL) could induce the gene expression of IL-6, ISG15, CXCL10, and IDO1 in uninfected Calu-3 cells (Figure 6D).

DISCUSSION

The increased systemic inflammation of SARS-CoV-2 leads to tissue injury. Herein, our GSH model study supported a differential immunometabolic response associated with inflammation and tissue injury. Our data also provide proof-of-principle evidence that the Delta variant is more pathogenic than Omicron, as seen in COVID-19 patients. This might be due to the altered host immunometabolic profiles. Additionally, this may offer evidence that increased systemic inflammation of SARS-CoV-2 respiratory infections can lead to inflammation in different tissues. Utilizing the GSH model, we showed differential systemic effects of Delta infection compared to Omicron despite comparable oral viral titers, but differences were seen in tissue compartments. The viral dynamics of Omicron in GSH follow the kinetics of the Delta variant,

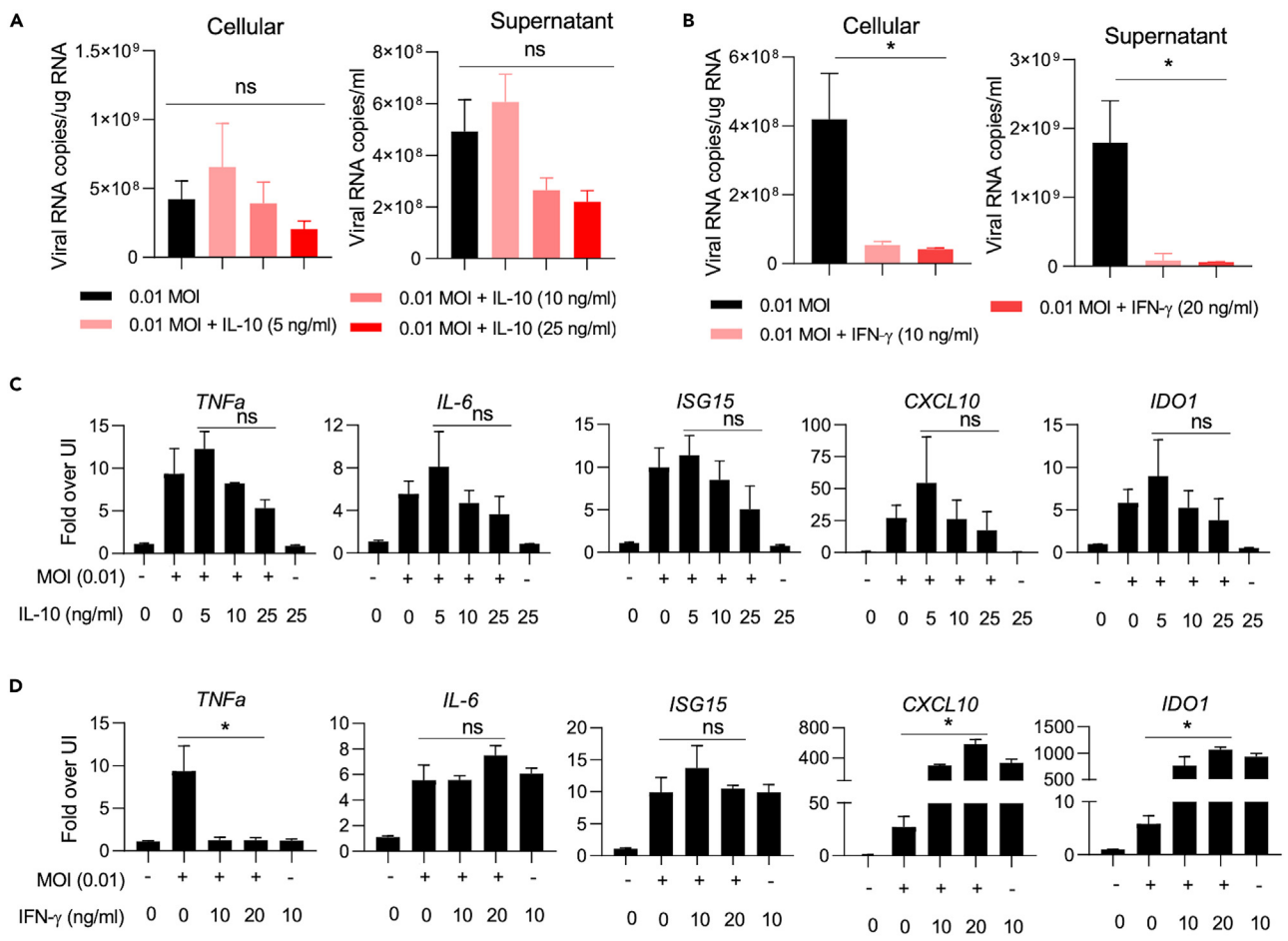

Figure 6. Effect of IL-10 and IFN-g on SARS-CoV-2 replication and SARS-CoV-2-induced cytokines, ISGs/chemokines, and IDO1 in Calu-3 cells

Calu-3 cells were pretreated with IL-10 (A) or IFN-g (B) for 1 h and infected with SARS-CoV-2 (delta variant) with 0.01 MOI for 48 h. RNA was isolated from cell lysate and culture supernatant and analyzed for viral RNA copies using E gene-specific primers and probes by RT-qPCR (A and B). Total cellular RNA was reverse transcribed to cDNA, and gene expression of host genes was analyzed by RT-qPCR (C and D). Data represent the mean ± SEM. *$p < 0.05$, 0.01 MOI vs. 0.01 MOI + IFN-γ. ns, non-significant.

which has relatively fewer viral RNA copies in respiratory tissues. We found that viral loads based on the E gene and subgenomic N gene copies in oral swabs and tissues for Delta and Omicron variants showed a positive correlation when compared. These findings suggest that there might be a relationship between potential tissue viral reservoirs and viral progression. Unlike the Delta variant, body weight loss was not observed in Omicron-infected GSH. Moreover, the Omicron variant had a lower impact on lung pathology than the Delta variant. These data suggested the differential systemic effects of Delta infection, compared to Omicron, despite comparable oral viral titers.[65,66]

The host immune response is critical in responding to viral infection by activating antiviral factors.[67,68] Clinical studies correlated SARS-CoV-2-mediated hyperactive immune response with cytokine storms leading to patient death.[17,69,70] Our findings of the low cytokine/chemokines/ISGs/metabolic enzymes expression in Omicron-infected GSH lung compared to Delta-infected lungs corroborated with the cytokine profile detected in COVID-19 patient blood samples.[71] A similar gene expression profile was observed in Calu-3 cells infected with Delta and Omicron variants. In Calu-3 cells, Delta variant replication kinetics was robust compared to the Omicron variant that correlated with the host gene expression profile.

Interestingly, the gene expression of the anti-inflammatory cytokine IL-10 was upregulated early in GSH lungs infected with the Delta variant compared to Omicron-infected lungs. It has been demonstrated that increased expression of IL-10 and IL-6 is a direct/indirect predictor of poor outcomes in COVID-19 severity.[72,73] The elevation of IL-10 is known to be involved in low antigen presentation and co-stimulation capacity of macrophages and dendritic cells to eliminate the virus during acute infection.[74] The higher expression of IL-10 may also be linked to the dampen hosts response to control inflammation and tissue damage concurrently with the production of IFN-γ as observed in COVID-19 patients.[75,76] This may support the notion that reducing inflammation and associated tissue damage may be more impactful than regulating infected cells directly. Similarly, the marked elevation of CXCL10 level is related to the development of hyperinflammatory responses, ARDS, and neurological complications and is associated with poor prognosis among COVID-19 patients.[77–79] It has been

observed that an effective early treatment for COVID-19 leads to restraints of the "cytokine storm", as well as reduction of CXCL10 levels.[80] The upregulation of CXCL10 in COVID-19 patients seems to be responsible for pulmonary edema and inflammation resulting in tissue injury.[79] CXCL10 being a Th1 chemokine,[81] its secretion is stimulated by IFN-γ from a wide range of cell types that includes monocytes, leukocytes, epithelial cells, and endothelial cells.[82] CXCL10 acts through its cognate receptor CXCR3 to drive the immune responses, and activation of these pathways leads to a hyperinflammatory state.[83,84] Therefore, strategies for modulation of the CXCL10–CXCR3 axis may be an effective therapeutic strategy to ameliorate SARS-CoV-2 mediated hyperinflammatory responses and the associated tissue insults in lungs.[85]

Immunometabolism regulates immune functions in both lymphoid and myeloid cells.[54] Several metabolic enzymes, including Arg1, iNOS, and IDO1, represent potential therapeutic targets in human diseases and regulate inflammation.[86] Arg1 is highly expressed in the liver and can regulate immune responses to infection.[26,87,88] Arg1 is also expressed in M2 macrophages, and its enzymatic activity depletes arginine, resulting in reduced nitric oxide (NO) generation by M1 macrophages by the action of iNOS.[53,88,89] NO is an essential metabolite that induces antiviral activity against RNA viruses, including SARS-CoV-2.[88,89] These indicated that the more pathogenic Delta variant utilizes the Arg1 pathway to reduce the availability of arginine to iNOS, which in turn reduces the production of NO. In contrast, Omicron was correlated with the low level of Arg1 and reduced lung damage. Further, the high expression of Arg1 in Delta-infected GSH lungs indicated that infiltrating immune cells, especially macrophages, are the significant source of Arg1 since SARS-CoV-2 infected Calu-3 (lung epithelial) cells failed to express the Arg1 gene and protein.

Another key metabolic enzyme, IDO1, depletes an essential amino acid, tryptophan, and generates kynurenine, known for its immunosuppressive action.[55,90] Kynurenine is one of the tryptophan metabolites that is highly elevated in Delta-infected GSH lungs. The Delta-infected GSH lungs exhibited increased levels of Arg1 and IDO1, indicating the involvement of immunometabolism pathways in SARS-CoV-2-mediated lung damage. This is supported by a clinical study in COVID-19 patients that reported the upregulation of the Arg1 gene, and it has been utilized as a diagnostic parameter in COVID-19 immunopathology.[21] Interestingly, the protein expression of Arg1 was elevated in GSH lungs upon Delta variant infection compared to Omicron infection and directly correlated with lung pathology. Additionally, the altered metabolic profiles of tryptophan (Trp) metabolic pathways in the lungs from GSH infected with Delta and Omicron variants proved that the IDO pathway is involved in SARS-CoV-2-induced pathology. Although the protein expression of IDO was not detected in Delta or Omicron-infected GSH lung tissues by human-specific anti-IDO antibody, increased Kyn to Trp ratio was a direct indicator of IDO activity. Interestingly, the elevated Arg1 activity induces tissue fibrosis by excessive collagen production.[26] The increased collagen staining in GSH lungs infected with the Delta variant correlated with an enhanced level of Arg1. Several contradictory reports exist on the persistence of lung fibrosis and tissue remodeling in hamster models of SARS-CoV-2.[91–95] While some studies found that lung fibrosis was not persistent in hamsters after the resolution of acute infection,[44] some suggested the presence of pulmonary fibrosis and tissue remodeling in hamsters post-recovery from acute illness.[91–95] The discrepancy between our study and published studies could be the time of analysis of the lung tissue fibrosis, where the published report studied tissue fibrosis at 31 DPI compared to our analysis at 10 DPI. Additionally, Frere et al.[44] used the wild-type SARS-CoV-2 isolate, whereas we reported the presence of tissue fibrosis in SARS-CoV-2 Delta (which was more pathogenic vs. wild-type virus) infected hamsters. On the other hand, Heydemann et al. recently showed lung fibrosis in SARS-CoV-2 infected hamsters at 14 DPI with the infiltration of M2 macrophages 91 that substantiates our findings with increased picrosirius staining along with the elevated expression of Arg1 in Delta infected hamster lungs. Furthermore, several other confounding factors may play a role, such as strain and viral titer used to infect the animals, age and sex of the animals, and any other comorbid conditions associated with infection and progressing to disease. Thus, more detailed studies are warranted to delineate the impact of different variants of SARS-CoV-2 and the timing of lung sampling to understand SARS-CoV-2 mediated lung fibrosis.

Further, amino acids originating from collagen metabolism, 4-hydroxyproline, *cis*-4-hydroxyproline, and alanine were downregulated. Our findings were corroborated by the decreased plasma level of 4-hydroxyproline reported in COVID-19 patients with an elevated level of IL-6.[28] The reduced level of hydroxyproline and alanine may imply that elevated collagen synthesis utilizes these amino acids or reduction in collagen degradation. Therefore, our study provided a novel insight to explore the direct involvement of Arg1/IDO1 in SARS-CoV-2 mediated lung pathology using Arg1/IDO1-specific inhibitors as therapeutics not only for SARS-CoV-2 but also for other respiratory virus-induced lung diseases and associated tissue fibrosis. Based on these observations, we can predict that either inhibition of IDO or Arg1 or together might be beneficial in controlling lung damage and maintaining immune homeostasis in COVID-19 patients. Otherwise, a good source of Trp supplement is necessary to maintain the essential amino acid pool to combat infection.

Finally, our metabolomics data supported the high uric acid level, the final product of purine catabolism, which is associated with compromised lung function during SARS-CoV-2 infection. The elevated uric acid level has been linked to asthma-like phenotypes upon exposure to environmental pollutants and allergens that trigger Th2 lymphocyte-mediated inflammatory responses in the mucosal tissue.[96] The involvement of uric acid has also been reported during respiratory viral infection that promotes a Th2 immune response.[97] Besides, an association has been clinically established between high serum uric acid levels and tissue hypoxia-induced pulmonary arterial hypertension and inflammation-induced lung damage.[98] Therefore, our findings indicate that the elevated uric acid levels in the lung tissues of GSH infected with SARS-CoV-2 Delta or Omicron could contribute to the long-term-associated asthma-like phenotype.[99] Since elevated uric acid levels have been implicated in lung pathology, the purine metabolic pathway could be explored as a novel therapeutic target for treating asthma-like pathology in COVID-19 patients.[100,101] In conclusion, our study provides novel insight into the differential immunopathogenesis and immunometabolism mediated by SARS-CoV-2 variants in GSH that offers novel therapeutic targets to mitigate SARS-CoV-2 virus-mediated lung pathology.

Limitations of the study

Although the GSH model closely recapitulates the lung disease pathophysiology with innate and adaptive immune responses as observed in COVID-19 patients, certain caveats should be considered while comparing them with humans, including (a) GSH do not develop ARDS,[102] (b) they do not succumb to the infection; and (c) due to less frequent use the research reagents required for immunophenotyping and protein profiling studies are not well developed for hamsters that limit specific immune response studies.[103] Due to these limitations, it is not feasible to perform a comprehensive immunophenotyping of the blood, lung tissues, bronchoalveolar lavage (BAL) fluids, etc. It is also difficult to confirm the changes observed at the transcript level translate at the protein level due to the unavailability of reagents to perform ELISA and signaling cascade.

However, the GSH model is widely used in coronavirus research due to the structural homology with the human ACE2 receptor, the principal host cell entry receptor for SARS-CoV-2. The disease manifestation of SARS-CoV-2 infected hamsters closely complements the upper and lower respiratory tract infection observed in humans.[104] The viral transmission from infected to naive hamsters follows a similar pattern observed in humans.[104] Additionally, in the lungs of SARS-CoV-2 infected hamsters, inflammatory solid response, infiltration of immune cells, and edema are reported.[105] GSH also develops humoral immune responses and neutralizing antibodies against SARS-CoV-2.[106] Apart from these, innate immune response mediated cytokine storm, lymphopenia, and impairment of the adaptive immune response in SARS-CoV-2 infected hamsters have been reported.[69,107] Finally, GSH mimics the age-dependent disease pathogenesis observed in COVID-19 patients.[108]

STAR★METHODS

Detailed methods are provided in the online version of this paper and include the following:

- KEY RESOURCES TABLE
- RESOURCE AVAILABILITY
  - Lead contact
  - Materials availability
  - Data and code availability
- EXPERIMENTAL MODEL AND STUDY PARTICIPANT DETAILS
  - Cell lines
  - Viral stocks
  - Study approval
- METHOD DETAILS
  - Hamster study
  - Hamsters infection
  - Cell culture
  - SARS-CoV-2 viral stocks
  - RNA isolation and RT-qPCR
  - Histology (H & E) and immunohistochemistry (IHC)
  - LC-MS metabolomic profile of hamster lung tissues
  - Calu-3 cells infection with SARS-CoV-2 variants
  - Western blotting
- QUANTIFICATION AND STATISTICAL ANALYSIS

SUPPLEMENTAL INFORMATION

Supplemental information can be found online at https://doi.org/10.1016/j.isci.2024.110501.

ACKNOWLEDGMENTS

We acknowledge the UNMC ABSL3 and BSL-3 core facility for allowing us to perform all *in vivo* and *in vitro* experiments involving SARS-CoV-2. This facility is administered by the office of the Vice-Chancellor for research and supported by the Nebraska Research Initiative (NRI). We acknowledge all the current and past members of Byrareddy's laboratory for helping to complete the experiments described in the manuscript. The authors acknowledge the biosafety leadership team and technical staff (Kristin M. Leland Wavrin and her Staff) from the Comparative Medicine, UNMC, for excellent experimental assistance. We thank the Metabolomics Core Facility, University of Iowa, Carver College of Medicine, Iowa, for metabolomic profile analysis. This work was partially supported by the National Institute of Allergy and Infectious Diseases grants R01 AI113883 and NIDA DA052845 (S.N.B.), the Philadelphia Foundation (Robert I. Jacobs Fund), Commonwealth of Pennsylvania COVID-19 funding, and the Kean Family Professorship (L.J.M.). S.N.B. acknowledges independent research and development (IRAD) funding from the National Strategic Research Institute (NSRI) and Nebraska Research Initiative (NRI) grants at the University of Nebraska and Otis Glebe Medical Research Foundation award. Eugene Kenney Memorial Fund to A.Acharya. UN acknowledges support from the Swedish Research Council grants 2021-00993 and 2021-01756.

AUTHOR CONTRIBUTIONS

S.N.B. and R.R. conceived the idea and designed the study. R.R., K.P., N.K., and R.G. performed experiments and acquired the data. S.C. performed histopathological scoring and helped to edit the manuscript. S.N.A. performed virological correlation in tissues and plasma. A.Ambikan. and U.N. analyzed and interpreted metabolomic data. RR wrote the original draft and thoroughly revised it by A.Acharya. and S.N.B. L.M. provided critical insights and edited the manuscript. S.N.B. supervised the study, acquired funding and extensive edits, and co-ordinated the manuscript. All authors read and approved the final version of the manuscript.

DECLARATION OF INTERESTS

The authors declared no competing interest.

Received: August 24, 2023
Revised: February 7, 2024
Accepted: July 10, 2024
Published: July 14, 2024

REFERENCES

1. V'Kovski, P., Kratzel, A., Steiner, S., Stalder, H., and Thiel, V. (2021). Coronavirus biology and replication: implications for SARS-CoV-2. Nat. Rev. Microbiol. *19*, 155–170. https://doi.org/10.1038/s41579-020-00468-6.
2. Del Rio, C., and Malani, P.N. (2020). COVID-19-New Insights on a Rapidly Changing Epidemic. JAMA *323*, 1339–1340. https://doi.org/10.1001/jama.2020.3072.
3. Edara, V.V., Norwood, C., Floyd, K., Lai, L., Davis-Gardner, M.E., Hudson, W.H., Mantus, G., Nyhoff, L.E., Adelman, M.W., Fineman, R., et al. (2021). Infection- and vaccine-induced antibody binding and neutralization of the B.1.351 SARS-CoV-2 variant. Cell Host Microbe *29*, 516–521.e3. https://doi.org/10.1016/j.chom.2021.03.009.
4. Hoffmann, M., Kleine-Weber, H., Schroeder, S., Kruger, N., Herrler, T., Erichsen, S., Schiergens, T.S., Herrler, G., Wu, N.H., Nitsche, A., et al. (2020). SARS-CoV-2 Cell Entry Depends on ACE2 and TMPRSS2 and Is Blocked by a Clinically Proven Protease Inhibitor. Cell *181*, 271–280.e8. https://doi.org/10.1016/j.cell.2020.02.052.
5. Rothan, H.A., and Byrareddy, S.N. (2020). The epidemiology and pathogenesis of coronavirus disease (COVID-19) outbreak. J. Autoimmun. *109*, 102433. https://doi.org/10.1016/j.jaut.2020.102433.
6. Saito, A., Irie, T., Suzuki, R., Maemura, T., Nasser, H., Uriu, K., Kosugi, Y., Shirakawa, K., Sadamasu, K., Kimura, I., et al. (2022). Enhanced fusogenicity and pathogenicity of SARS-CoV-2 Delta P681R mutation. Nature *602*, 300–306. https://doi.org/10.1038/s41586-021-04266-9.
7. Lopez Bernal, J., Andrews, N., Gower, C., Gallagher, E., Simmons, R., Thelwall, S., Stowe, J., Tessier, E., Groves, N., Dabrera, G., et al. (2021). Effectiveness of Covid-19 Vaccines against the B.1.617.2 (Delta) Variant. N. Engl. J. Med. *385*, 585–594. https://doi.org/10.1056/NEJMoa2108891.
8. Mohandas, S., Yadav, P.D., Shete, A., Nyayanit, D., Sapkal, G., Lole, K., and Gupta, N. (2021). SARS-CoV-2 Delta Variant Pathogenesis and Host Response in Syrian Hamsters. Viruses *13*, 1773. https://doi.org/10.3390/v13091773.
9. Mlcochova, P., Kemp, S.A., Dhar, M.S., Papa, G., Meng, B., Ferreira, I., Datir, R., Collier, D.A., Albecka, A., Singh, S., et al. (2021). SARS-CoV-2 B.1.617.2 Delta variant replication and immune evasion. Nature *599*, 114–119. https://doi.org/10.1038/s41586-021-03944-y.
10. Tegally, H., Moir, M., Everatt, J., Giovanetti, M., Scheepers, C., Wilkinson, E., Subramoney, K., Makatini, Z., Moyo, S., Amoako, D.G., et al. (2022). Emergence of SARS-CoV-2 Omicron lineages BA.4 and BA.5 in South Africa. Nat. Med. *28*, 1785–1790. https://doi.org/10.1038/s41591-022-01911-2.
11. Mohandas, S., Yadav, P.D., Sapkal, G., Shete, A.M., Deshpande, G., Nyayanit, D.A., Patil, D., Kadam, M., Kumar, A., Mote, C., and Jain, R. (2022). Pathogenicity of SARS-CoV-2 Omicron (R346K) variant in Syrian hamsters and its cross-neutralization with different variants of concern. EBioMedicine *79*, 103997. https://doi.org/10.1016/j.ebiom.2022.103997.
12. Mishra, A.R., Nayak, D., and Byrareddy, S.N. (2022). Are we moving toward ending SARS-CoV-2? J. Med. Virol. *94*, 2921–2924. https://doi.org/10.1002/jmv.27722.
13. Van Egeren, D., Stoddard, M., White, L.F., Hochberg, N.S., Rogers, M.S., Zetter, B., Joseph-McCarthy, D., and Chakravarty, A. (2023). Vaccines Alone Cannot Slow the Evolution of SARS-CoV-2. Vaccines (Basel) *11*, 853. https://doi.org/10.3390/vaccines11040853.
14. Wong, L.R., and Perlman, S. (2022). Immune dysregulation and immunopathology induced by SARS-CoV-2 and related coronaviruses - are we our own worst enemy? Nat. Rev. Immunol. *22*, 47–56. https://doi.org/10.1038/s41577-021-00656-2.
15. Olwenyi, O.A., Dyavar, S.R., Acharya, A., Podany, A.T., Fletcher, C.V., Ng, C.L., Reid, S.P., and Byrareddy, S.N. (2020). Immuno-epidemiology and pathophysiology of coronavirus disease 2019 (COVID-19). J. Mol. Med. *98*, 1369–1383. https://doi.org/10.1007/s00109-020-01961-4.
16. Devadoss, D., Acharya, A., Manevski, M., Houserova, D., Cioffi, M.D., Pandey, K., Nair, M., Chapagain, P., Mirsaeidi, M., Borchert, G.M., et al. (2022). Immunomodulatory LncRNA on antisense strand of ICAM-1 augments SARS-CoV-2 infection-associated airway mucoinflammatory phenotype. iScience *25*, 104685. https://doi.org/10.1016/j.isci.2022.104685.
17. Wang, J., Jiang, M., Chen, X., and Montaner, L.J. (2020). Cytokine storm and leukocyte changes in mild versus severe SARS-CoV-2 infection: Review of 3939 COVID-19 patients in China and emerging pathogenesis and therapy concepts. J. Leukoc. Biol. *108*, 17–41. https://doi.org/10.1002/JLB.3COVR0520-272R.
18. Palmer, C.S. (2022). Innate metabolic responses against viral infections. Nat. Metab. *4*, 1245–1259. https://doi.org/10.1038/s42255-022-00652-3.
19. Ambikan, A.T., Yang, H., Krishnan, S., Svensson Akusjarvi, S., Gupta, S., Lourda, M., Sperk, M., Arif, M., Zhang, C., Nordqvist, H., et al. (2022). Multi-omics personalized network analyses highlight progressive disruption of central metabolism associated with COVID-19 severity. Cell Syst. *13*, 665–681. https://doi.org/10.1016/j.cels.2022.06.006.
20. Krishnan, S., Nordqvist, H., Ambikan, A.T., Gupta, S., Sperk, M., Svensson-Akusjarvi, S., Mikaeloff, F., Benfeitas, R., Saccon, E., Ponnan, S.M., et al. (2021). Metabolic Perturbation Associated With COVID-19 Disease Severity and SARS-CoV-2 Replication. Mol. Cell. Proteomics *20*, 100159. https://doi.org/10.1016/j.mcpro.2021.100159.
21. Derakhshani, A., Hemmat, N., Asadzadeh, Z., Ghaseminia, M., Shadbad, M.A., Jadideslam, G., Silvestris, N., Racanelli, V., and Baradaran, B. (2021). Arginase 1 (*Arg1*) as an Up-Regulated Gene in COVID-19 Patients: A Promising Marker in COVID-19 Immunopathy. J. Clin. Med. *10*, 1051. https://doi.org/10.3390/jcm10051051.
22. Guo, L., Schurink, B., Roos, E., Nossent, E.J., Duitman, J.W., Vlaar, A.P., van der Valk, P., Vaz, F.M., Yeh, S.R., Geeraerts, Z., et al. (2022). Indoleamine 2,3-dioxygenase (IDO)-1 and IDO-2 activity and severe course of COVID-19. J. Pathol. *256*, 256–261. https://doi.org/10.1002/path.5842.
23. Islam, H., Chamberlain, T.C., Mui, A.L., and Little, J.P. (2021). Elevated Interleukin-10 Levels in COVID-19: Potentiation of Pro-Inflammatory Responses or Impaired Anti-Inflammatory Action? Front. Immunol. *12*, 677008. https://doi.org/10.3389/fimmu.2021.677008.

24. Steen, E.H., Wang, X., Balaji, S., Butte, M.J., Bollyky, P.L., and Keswani, S.G. (2020). The Role of the Anti-Inflammatory Cytokine Interleukin-10 in Tissue Fibrosis. Adv. Wound Care *9*, 184–198. https://doi.org/10.1089/wound.2019.1032.
25. Zdrenghea, M.T., Makrinioti, H., Muresan, A., Johnston, S.L., and Stanciu, L.A. (2015). The role of macrophage IL-10/innate IFN interplay during virus-induced asthma. Rev. Med. Virol. *25*, 33–49. https://doi.org/10.1002/rmv.1817.
26. Pesce, J.T., Ramalingam, T.R., Mentink-Kane, M.M., Wilson, M.S., El Kasmi, K.C., Smith, A.M., Thompson, R.W., Cheever, A.W., Murray, P.J., and Wynn, T.A. (2009). Arginase-1-expressing macrophages suppress Th2 cytokine-driven inflammation and fibrosis. PLoS Pathog. *5*, e1000371. https://doi.org/10.1371/journal.ppat.1000371.
27. Dufour, I., Werion, A., Belkhir, L., Wisniewska, A., Perrot, M., De Greef, J., Schmit, G., Yombi, J.C., Wittebole, X., Laterre, P.F., et al. (2021). Serum uric acid, disease severity and outcomes in COVID-19. Crit. Care *25*, 212. https://doi.org/10.1186/s13054-021-03616-3.
28. Masoodi, M., Peschka, M., Schmiedel, S., Haddad, M., Frye, M., Maas, C., Lohse, A., Huber, S., Kirchhof, P., Nofer, J.R., and Renne, T. (2022). Disturbed lipid and amino acid metabolisms in COVID-19 patients. J. Mol. Med. *100*, 555–568. https://doi.org/10.1007/s00109-022-02177-4.
29. Bao, L., Deng, W., Huang, B., Gao, H., Liu, J., Ren, L., Wei, Q., Yu, P., Xu, Y., Qi, F., et al. (2020). The pathogenicity of SARS-CoV-2 in hACE2 transgenic mice. Nature *583*, 830–833. https://doi.org/10.1038/s41586-020-2312-y.
30. Imai, M., Iwatsuki-Horimoto, K., Hatta, M., Loeber, S., Halfmann, P.J., Nakajima, N., Watanabe, T., Ujie, M., Takahashi, K., Ito, M., et al. (2020). Syrian hamsters as a small animal model for SARS-CoV-2 infection and countermeasure development. Proc. Natl. Acad. Sci. USA *117*, 16587–16595. https://doi.org/10.1073/pnas.2009799117.
31. Pandey, K., Acharya, A., Mohan, M., Ng, C.L., Reid, S.P., and Byrareddy, S.N. (2021). Animal models for SARS-CoV-2 research: A comprehensive literature review. Transbound. Emerg. Dis. *68*, 1868–1885. https://doi.org/10.1111/tbed.13907.
32. Halfmann, P.J., Iida, S., Iwatsuki-Horimoto, K., Maemura, T., Kiso, M., Scheaffer, S.M., Darling, T.L., Joshi, A., Loeber, S., Singh, G., et al. (2022). SARS-CoV-2 Omicron virus causes attenuated disease in mice and hamsters. Nature *603*, 687–692. https://doi.org/10.1038/s41586-022-04441-6.
33. Ackermann, M., Verleden, S.E., Kuehnel, M., Haverich, A., Welte, T., Laenger, F., Vanstapel, A., Werlein, C., Stark, H., Tzankov, A., et al. (2020). Pulmonary Vascular Endothelialitis, Thrombosis, and Angiogenesis in Covid-19. N. Engl. J. Med. *383*, 120–128. https://doi.org/10.1056/NEJMoa2015432.
34. Matthay, M.A., Leligdowicz, A., and Liu, K.D. (2020). Biological Mechanisms of COVID-19 Acute Respiratory Distress Syndrome. Am. J. Respir. Crit. Care Med. *202*, 1489–1491. https://doi.org/10.1164/rccm.202009-3629ED.
35. Rajaiah, R., Abhilasha, K.V., Shekar, M.A., Vogel, S.N., and Vishwanath, B.S. (2020). Evaluation of mechanisms of action of re-purposed drugs for treatment of COVID-19. Cell. Immunol. *358*, 104240. https://doi.org/10.1016/j.cellimm.2020.104240.
36. Rothan, H.A., Acharya, A., Reid, S.P., Kumar, M., and Byrareddy, S.N. (2020). Molecular Aspects of COVID-19 Differential Pathogenesis. Pathogens *9*, 538. https://doi.org/10.3390/pathogens9070538.
37. Kumar, S., Thambiraja, T.S., Karuppanan, K., and Subramaniam, G. (2022). Omicron and Delta variant of SARS-CoV-2: A comparative computational study of spike protein. J. Med. Virol. *94*, 1641–1649. https://doi.org/10.1002/jmv.27526.
38. Kannan, S.R., Spratt, A.N., Cohen, A.R., Naqvi, S.H., Chand, H.S., Quinn, T.P., Lorson, C.L., Byrareddy, S.N., and Singh, K. (2021). Evolutionary analysis of the Delta and Delta Plus variants of the SARS-CoV-2 viruses. J. Autoimmun. *124*, 102715. https://doi.org/10.1016/j.jaut.2021.102715.
39. Kannan, S.R., Spratt, A.N., Sharma, K., Chand, H.S., Byrareddy, S.N., and Singh, K. (2022). Omicron SARS-CoV-2 variant: Unique features and their impact on pre-existing antibodies. J. Autoimmun. *126*, 102779. https://doi.org/10.1016/j.jaut.2021.102779.
40. Usai, C., Mateu, L., Brander, C., Vergara-Alert, J., and Segales, J. (2023). Animal models to study the neurological manifestations of the post-COVID-19 condition. Lab Anim. *52*, 202–210. https://doi.org/10.1038/s41684-023-01231-z.
41. Braxton, A.M., Creisher, P.S., Ruiz-Bedoya, C.A., Mulka, K.R., Dhakal, S., Ordonez, A.A., Beck, S.E., Jain, S.K., and Villano, J.S. (2021). Hamsters as a Model of Severe Acute Respiratory Syndrome Coronavirus-2. Comp. Med. *71*, 398–410. https://doi.org/10.30802/AALAS-CM-21-000036.
42. Schmitz, A.J., Turner, J.S., Liu, Z., Zhou, J.Q., Aziati, I.D., Chen, R.E., Joshi, A., Bricker, T.L., Darling, T.L., Adelsberg, D.C., et al. (2021). A vaccine-induced public antibody protects against SARS-CoV-2 and emerging variants. Immunity *54*, 2159–2166. https://doi.org/10.1016/j.immuni.2021.08.013.
43. O'Donnell, K.L., Pinski, A.N., Clancy, C.S., Gourdine, T., Shifflett, K., Fletcher, P., Messaoudi, I., and Marzi, A. (2021). Pathogenic and transcriptomic differences of emerging SARS-CoV-2 variants in the Syrian golden hamster model. EBioMedicine *73*, 103675. https://doi.org/10.1016/j.ebiom.2021.103675.
44. Frere, J.J., Serafini, R.A., Pryce, K.D., Zazhytska, M., Oishi, K., Golynker, I., Panis, M., Zimering, J., Horiuchi, S., Hoagland, D.A., et al. (2022). SARS-CoV-2 infection in hamsters and humans results in lasting and unique systemic perturbations after recovery. Sci. Transl. Med. *14*, eabq3059. https://doi.org/10.1126/scitranslmed.abq3059.
45. Minton, K. (2022). Mechanistic insights into Long COVID in hamsters. Nat. Rev. Immunol. *22*, 463. https://doi.org/10.1038/s41577-022-00757-6.
46. Ragab, D., Salah Eldin, H., Taeimah, M., Khattab, R., and Salem, R. (2020). The COVID-19 Cytokine Storm; What We Know So Far. Front. Immunol. *11*, 1446. https://doi.org/10.3389/fimmu.2020.01446.
47. Ruan, Q., Yang, K., Wang, W., Jiang, L., and Song, J. (2020). Clinical predictors of mortality due to COVID-19 based on an analysis of data of 150 patients from Wuhan, China. Intensive Care Med. *46*, 846–848. https://doi.org/10.1007/s00134-020-05991-x.
48. Xu, Z., Shi, L., Wang, Y., Zhang, J., Huang, L., Zhang, C., Liu, S., Zhao, P., Liu, H., Zhu, L., et al. (2020). Pathological findings of COVID-19 associated with acute respiratory distress syndrome. Lancet Respir. Med. *8*, 420–422. https://doi.org/10.1016/S2213-2600(20)30076-X.
49. Crosse, K.M., Monson, E.A., Beard, M.R., and Helbig, K.J. (2018). Interferon-Stimulated Genes as Enhancers of Antiviral Innate Immune Signaling. J. Innate Immun. *10*, 85–93. https://doi.org/10.1159/000484258.
50. Kelly-Scumpia, K.M., Scumpia, P.O., Delano, M.J., Weinstein, J.S., Cuenca, A.G., Wynn, J.L., and Moldawer, L.L. (2010). Type I interferon signaling in hematopoietic cells is required for survival in mouse polymicrobial sepsis by regulating CXCL10. J. Exp. Med. *207*, 319–326. https://doi.org/10.1084/jem.20091959.
51. Marques, R.E., Guabiraba, R., Russo, R.C., and Teixeira, M.M. (2013). Targeting CCL5 in inflammation. Expert Opin. Ther. Targets *17*, 1439–1460. https://doi.org/10.1517/14728222.2013.837886.
52. Bogdan, C. (2001). Nitric oxide and the immune response. Nat. Immunol. *2*, 907–916. https://doi.org/10.1038/ni1001-907.
53. El-Gayar, S., Thuring-Nahler, H., Pfeilschifter, J., Rollinghoff, M., and Bogdan, C. (2003). Translational control of inducible nitric oxide synthase by IL-13 and arginine availability in inflammatory macrophages. J. Immunol. *171*, 4561–4568. https://doi.org/10.4049/jimmunol.171.9.4561.
54. Godfrey, W.H., and Kornberg, M.D. (2020). The Role of Metabolic Enzymes in the Regulation of Inflammation. Metabolites *10*, 426. https://doi.org/10.3390/metabo10110426.
55. Munn, D.H., Zhou, M., Attwood, J.T., Bondarev, I., Conway, S.J., Marshall, B., Brown, C., and Mellor, A.L. (1998). Prevention of allogeneic fetal rejection by tryptophan catabolism. Science *281*, 1191–1193. https://doi.org/10.1126/science.281.5380.1191.
56. Freyberg, Z., and Harvill, E.T. (2017). Pathogen manipulation of host metabolism: A common strategy for immune evasion. PLoS Pathog. *13*, e1006669. https://doi.org/10.1371/journal.ppat.1006669.
57. Straub, R.H. (2014). Interaction of the endocrine system with inflammation: a function of energy and volume regulation. Arthritis Res. Ther. *16*, 203. https://doi.org/10.1186/ar4484.
58. Wasinski, F., Gregnani, M.F., Ornellas, F.H., Bacurau, A.V., Camara, N.O., Araujo, R.C., and Bacurau, R.F. (2014). Lymphocyte glucose and glutamine metabolism as targets of the anti-inflammatory and immunomodulatory effects of exercise. Mediators Inflamm. *2014*, 326803. https://doi.org/10.1155/2014/326803.
59. Kanova, M., and Kohout, P. (2021). Tryptophan: A Unique Role in the Critically Ill. Int. J. Mol. Sci. *22*, 11714. https://doi.org/10.3390/ijms222111714.
60. Krupa, A., and Kowalska, I. (2021). The Kynurenine Pathway-New Linkage between Innate and Adaptive Immunity in Autoimmune Endocrinopathies. Int. J. Mol. Sci. *22*, 9879. https://doi.org/10.3390/ijms22189879.

61. de Paz-Lugo, P., Lupianez, J.A., and Melendez-Hevia, E. (2018). High glycine concentration increases collagen synthesis by articular chondrocytes in vitro: acute glycine deficiency could be an important cause of osteoarthritis. Amino Acids *50*, 1357–1365. https://doi.org/10.1007/s00726-018-2611-x.
62. Oldham, W.M., Clish, C.B., Yang, Y., and Loscalzo, J. (2015). Hypoxia-Mediated Increases in L-2-hydroxyglutarate Coordinate the Metabolic Response to Reductive Stress. Cell Metab. *22*, 291–303. https://doi.org/10.1016/j.cmet.2015.06.021.
63. Bhattacharyya, A., Chattopadhyay, R., Mitra, S., and Crowe, S.E. (2014). Oxidative stress: an essential factor in the pathogenesis of gastrointestinal mucosal diseases. Physiol. Rev. *94*, 329–354. https://doi.org/10.1152/physrev.00040.2012.
64. Dhar, S.K., Vishnupriyan, K., Damodar, S., Gujar, S., and Das, M. (2021). IL-6 and IL-10 as predictors of disease severity in COVID-19 patients: results from meta-analysis and regression. Heliyon *7*, e06155. https://doi.org/10.1016/j.heliyon.2021.e06155.
65. Li, Q., Liu, X., Li, L., Hu, X., Cui, G., Sun, R., Zhang, D., Li, J., Li, Y., Zhang, Y., et al. (2022). Comparison of clinical characteristics between SARS-CoV-2 Omicron variant and Delta variant infections in China. Front. Med. *9*, 944909. https://doi.org/10.3389/fmed.2022.944909.
66. Yang, W., Yang, S., Wang, L., Zhou, Y., Xin, Y., Li, H., Mu, W., Wu, Q., Xu, L., Zhao, M., et al. (2022). Clinical characteristics of 310 SARS-CoV-2 Omicron variant patients and comparison with Delta and Beta variant patients in China. Virol. Sin. *37*, 704–715. https://doi.org/10.1016/j.virs.2022.07.014.
67. Kasuga, Y., Zhu, B., Jang, K.J., and Yoo, J.S. (2021). Innate immune sensing of coronavirus and viral evasion strategies. Exp. Mol. Med. *53*, 723–736. https://doi.org/10.1038/s12276-021-00602-1.
68. Kikkert, M. (2020). Innate Immune Evasion by Human Respiratory RNA Viruses. J. Innate Immun. *12*, 4–20. https://doi.org/10.1159/000503030.
69. Mehta, P., McAuley, D.F., Brown, M., Sanchez, E., Tattersall, R.S., Manson, J.J., and Hlh Across Speciality Collaboration, U.K. (2020). COVID-19: consider cytokine storm syndromes and immunosuppression. Lancet *395*, 1033–1034. https://doi.org/10.1016/S0140-6736(20)30628-0.
70. Pedersen, S.F., and Ho, Y.C. (2020). SARS-CoV-2: a storm is raging. J. Clin. Invest. *130*, 2202–2205. https://doi.org/10.1172/JCI137647.
71. Lebedeva, A., Molodtsov, I., Anisimova, A., Berestovskaya, A., Dukhin, O., Elizarova, A., Fitzgerald, W., Fomina, D., Glebova, K., Ivanova, O., et al. (2022). Comprehensive Cytokine Profiling of Patients with COVID-19 Receiving Tocilizumab Therapy. Int. J. Mol. Sci. *23*, 7937. https://doi.org/10.3390/ijms23147937.
72. Han, H., Ma, Q., Li, C., Liu, R., Zhao, L., Wang, W., Zhang, P., Liu, X., Gao, G., Liu, F., et al. (2020). Profiling serum cytokines in COVID-19 patients reveals IL-6 and IL-10 are disease severity predictors. Emerg. Microbes Infect. *9*, 1123–1130. https://doi.org/10.1080/22221751.2020.1770129.
73. Zhao, Y., Qin, L., Zhang, P., Li, K., Liang, L., Sun, J., Xu, B., Dai, Y., Li, X., Zhang, C., et al. (2020). Longitudinal COVID-19 profiling associates IL-1RA and IL-10 with disease severity and RANTES with mild disease. JCI Insight *5*, e139834. https://doi.org/10.1172/jci.insight.139834.
74. Serjeant, G.R., Mason, K.P., and Serjeant, B.E. (1980). Negro alpha-thalassaemia: genetic studies in homozygous sickle cell disease. J. Med. Genet. *17*, 281–284. https://doi.org/10.1136/jmg.17.4.281.
75. Blanco-Melo, D., Nilsson-Payant, B.E., Liu, W.C., Uhl, S., Hoagland, D., Moller, R., Jordan, T.X., Oishi, K., Panis, M., Sachs, D., et al. (2020). Imbalanced Host Response to SARS-CoV-2 Drives Development of COVID-19. Cell *181*, 1036–1045.e9. https://doi.org/10.1016/j.cell.2020.04.026.
76. Zhou, Z., Ren, L., Zhang, L., Zhong, J., Xiao, Y., Jia, Z., Guo, L., Yang, J., Wang, C., Jiang, S., et al. (2020). Heightened Innate Immune Responses in the Respiratory Tract of COVID-19 Patients. Cell Host Microbe *27*, 883–890.e2. https://doi.org/10.1016/j.chom.2020.04.017.
77. Gudowska-Sawczuk, M., and Mroczko, B. (2022). What Is Currently Known about the Role of CXCL10 in SARS-CoV-2 Infection? Int. J. Mol. Sci. *23*, 3673. https://doi.org/10.3390/ijms23073673.
78. Huang, C., Wang, Y., Li, X., Ren, L., Zhao, J., Hu, Y., Zhang, L., Fan, G., Xu, J., Gu, X., et al. (2020). Clinical features of patients infected with 2019 novel coronavirus in Wuhan, China. Lancet *395*, 497–506. https://doi.org/10.1016/S0140-6736(20)30183-5.
79. Julian, D.R., Kazakoff, M.A., Patel, A., Jaynes, J., Willis, M.S., and Yates, C.C. (2021). Chemokine-Based Therapeutics for the Treatment of Inflammatory and Fibrotic Convergent Pathways in COVID-19. Curr. Pathobiol. Rep. *9*, 93–105. https://doi.org/10.1007/s40139-021-00226-0.
80. Noreen, S., Maqbool, I., and Madni, A. (2021). Dexamethasone: Therapeutic potential, risks, and future projection during COVID-19 pandemic. Eur. J. Pharmacol. *894*, 173854. https://doi.org/10.1016/j.ejphar.2021.173854.
81. Liang, R., Chen, S., Jin, Y., Tao, L., Ji, W., Zhu, P., Li, D., Zhang, Y., Zhang, W., and Duan, G. (2022). The CXCL10/CXCR3 Axis Promotes Disease Pathogenesis in Mice upon CVA2 Infection. Microbiol. Spectr. *10*, e0230721. https://doi.org/10.1128/spectrum.02307-21.
82. Çelik, N., Celik, O., Laloglu, E., and Ozkaya, A. (2023). The CXCL9/10/11-CXCR3 axis as a predictor of COVID-19 progression: a prospective, case-control study. Rev. Soc. Bras. Med. Trop. *56*, e01282023. https://doi.org/10.1590/0037-8682-0128-2023.
83. Petrisko, T.J., Bloemer, J., Pinky, P.D., Srinivas, S., Heslin, R.T., Du, Y., Setti, S.E., Hong, H., Suppiramaniam, V., Konat, G.W., and Reed, M.N. (2020). Neuronal CXCL10/CXCR3 Axis Mediates the Induction of Cerebral Hyperexcitability by Peripheral Viral Challenge. Front. Neurosci. *14*, 220. https://doi.org/10.3389/fnins.2020.00220.
84. Kong, Y.F., Sha, W.L., Wu, X.B., Zhao, L.X., Ma, L.J., and Gao, Y.J. (2021). CXCL10/CXCR3 Signaling in the DRG Exacerbates Neuropathic Pain in Mice. Neurosci. Bull. *37*, 339–352. https://doi.org/10.1007/s12264-020-00608-1.
85. Ichikawa, A., Kuba, K., Morita, M., Chida, S., Tezuka, H., Hara, H., Sasaki, T., Ohteki, T., Ranieri, V.M., dos Santos, C.C., et al. (2013). CXCL10-CXCR3 enhances the development of neutrophil-mediated fulminant lung injury of viral and nonviral origin. Am. J. Respir. Crit. Care Med. *187*, 65–77. https://doi.org/10.1164/rccm.201203-0508OC.
86. Patel, C.H., Leone, R.D., Horton, M.R., and Powell, J.D. (2019). Targeting metabolism to regulate immune responses in autoimmunity and cancer. Nat. Rev. Drug Discov. *18*, 669–688. https://doi.org/10.1038/s41573-019-0032-5.
87. Burrack, K.S., Tan, J.J., McCarthy, M.K., Her, Z., Berger, J.N., Ng, L.F., and Morrison, T.E. (2015). Myeloid Cell Arg1 Inhibits Control of Arthritogenic Alphavirus Infection by Suppressing Antiviral T Cells. PLoS Pathog. *11*, e1005191. https://doi.org/10.1371/journal.ppat.1005191.
88. Caldwell, R.W., Rodriguez, P.C., Toque, H.A., Narayanan, S.P., and Caldwell, R.B. (2018). Arginase: A Multifaceted Enzyme Important in Health and Disease. Physiol. Rev. *98*, 641–665. https://doi.org/10.1152/physrev.00037.2016.
89. Tatum, D., Taghavi, S., Houghton, A., Stover, J., Toraih, E., and Duchesne, J. (2020). Neutrophil-to-Lymphocyte Ratio and Outcomes in Louisiana COVID-19 Patients. Shock *54*, 652–658. https://doi.org/10.1097/SHK.0000000000001585.
90. Triplett, T.A., Garrison, K.C., Marshall, N., Donkor, M., Blazeck, J., Lamb, C., Qerqez, A., Dekker, J.D., Tanno, Y., Lu, W.C., et al. (2018). Reversal of indoleamine 2,3-dioxygenase-mediated cancer immune suppression by systemic kynurenine depletion with a therapeutic enzyme. Nat. Biotechnol. *36*, 758–764. https://doi.org/10.1038/nbt.4180.
91. Heydemann, L., Ciurkiewicz, M., Beythien, G., Becker, K., Schughart, K., Stanelle-Bertram, S., Schaumburg, B., Mounogou-Kouassi, N., Beck, S., Zickler, M., et al. (2023). Hamster model for post-COVID-19 alveolar regeneration offers an opportunity to understand post-acute sequelae of SARS-CoV-2. Nat. Commun. *14*, 3267. https://doi.org/10.1038/s41467-023-39049-5.
92. Kolloli, A., Ramasamy, S., Kumar, R., Nisa, A., Kaplan, G., and Subbian, S. (2023). A phosphodiesterase-4 inhibitor reduces lung inflammation and fibrosis in a hamster model of SARS-CoV-2 infection. Front. Immunol. *14*, 1270414. https://doi.org/10.3389/fimmu.2023.1270414.
93. Briand, F., Sencio, V., Robil, C., Heumel, S., Deruyter, L., Machelart, A., Barthelemy, J., Bogard, G., Hoffmann, E., Infanti, F., et al. (2022). Diet-Induced Obesity and NASH Impair Disease Recovery in SARS-CoV-2-Infected Golden Hamsters. Viruses *14*, 2067. https://doi.org/10.3390/v14092067.
94. Bogard, G., Barthelemy, J., Hantute-Ghesquier, A., Sencio, V., Brito-Rodrigues, P., Seron, K., Robil, C., Flourens, A., Pinet, F., Eberle, D., et al. (2023). SARS-CoV-2 infection induces persistent adipose tissue damage in aged golden Syrian hamsters. Cell Death Dis. *14*, 75. https://doi.org/10.1038/s41419-023-05574-w.
95. Bagato, O., Balkema-Buschmann, A., Todt, D., Weber, S., Gomer, A., Qu, B., Miskey, C., Ivics, Z., Mettenleiter, T.C., Finke, S., et al. (2024). Spatiotemporal analysis of SARS-CoV-2 infection reveals an expansive wave of monocyte-derived macrophages associated with vascular damage and virus clearance in hamster lungs. Microbiol. Spectr. *12*, e0246923. https://doi.org/10.1128/spectrum.02469-23.
96. Gold, M.J., Hiebert, P.R., Park, H.Y., Stefanowicz, D., Le, A., Starkey, M.R.,

Deane, A., Brown, A.C., Liu, G., Horvat, J.C., et al. (2016). Mucosal production of uric acid by airway epithelial cells contributes to particulate matter-induced allergic sensitization. Mucosal Immunol. *9*, 809–820. https://doi.org/10.1038/mi.2015.104.

97. Fonseca, W., Malinczak, C.A., Schuler, C.F., Best, S.K.K., Rasky, A.J., Morris, S.B., Cui, T.X., Popova, A.P., and Lukacs, N.W. (2020). Uric acid pathway activation during respiratory virus infection promotes Th2 immune response via innate cytokine production and ILC2 accumulation. Mucosal Immunol. *13*, 691–701. https://doi.org/10.1038/s41385-020-0264-z.
98. Sahana, K., and Sivaranjani, H. (2022). Uric Acid: A Mirror to the Lungs in COPD. J. Assoc. Physicians India *70*, 11–12.
99. Mantovani, A., Morrone, M.C., Patrono, C., Santoro, M.G., Schiaffino, S., Remuzzi, G., and Bussolati, G.; Covid-19 Commission of the Accademia Nazionale dei Lincei (2022). Long Covid: where we stand and challenges ahead. Cell Death Differ. *29*, 1891–1900. https://doi.org/10.1038/s41418-022-01052-6.
100. Ravi, A., Goorsenberg, A.W.M., Dijkhuis, A., Dierdorp, B.S., Dekker, T., van Weeghel, M., Sabogal Pineros, Y.S., Shah, P.L., Ten Hacken, N.H.T., Annema, J.T., et al. (2021). Metabolic differences between bronchial epithelium from healthy individuals and patients with asthma and the effect of bronchial thermoplasty. J. Allergy Clin. Immunol. *148*, 1236–1248. https://doi.org/10.1016/j.jaci.2020.12.653.
101. Yu, M., Cui, F.X., Jia, H.M., Zhou, C., Yang, Y., Zhang, H.W., Ding, G., and Zou, Z.M. (2016). Aberrant purine metabolism in allergic asthma revealed by plasma metabolomics. J. Pharm. Biomed. Anal. *120*, 181–189. https://doi.org/10.1016/j.jpba.2015.12.018.
102. Shou, S., Liu, M., Yang, Y., Kang, N., Song, Y., Tan, D., Liu, N., Wang, F., Liu, J., and Xie, Y. (2021). Animal Models for COVID-19: Hamsters, Mouse, Ferret, Mink, Tree Shrew, and Non-human Primates. Front. Microbiol. *12*, 626553. https://doi.org/10.3389/fmicb.2021.626553.
103. Cleary, S.J., Pitchford, S.C., Amison, R.T., Carrington, R., Robaina Cabrera, C.L., Magnen, M., Looney, M.R., Gray, E., and Page, C.P. (2020). Animal models of mechanisms of SARS-CoV-2 infection and COVID-19 pathology. Br. J. Pharmacol. *177*, 4851–4865. https://doi.org/10.1111/bph.15143.
104. Chan, J.F., Zhang, A.J., Yuan, S., Poon, V.K., Chan, C.C., Lee, A.C., Chan, W.M., Fan, Z., Tsoi, H.W., Wen, L., et al. (2020). Simulation of the Clinical and Pathological Manifestations of Coronavirus Disease 2019 (COVID-19) in a Golden Syrian Hamster Model: Implications for Disease Pathogenesis and Transmissibility. Clin. Infect. Dis. *71*, 2428–2446. https://doi.org/10.1093/cid/ciaa325.
105. Boudewijns, R., Thibaut, H.J., Kaptein, S.J.F., Li, R., Vergote, V., Seldeslachts, L., Van Weyenbergh, J., De Keyzer, C., Bervoets, L., Sharma, S., et al. (2020). STAT2 signaling restricts viral dissemination but drives severe pneumonia in SARS-CoV-2 infected hamsters. Nat. Commun. *11*, 5838. https://doi.org/10.1038/s41467-020-19684-y.
106. Casel, M.A.B., Rollon, R.G., and Choi, Y.K. (2021). Experimental Animal Models of Coronavirus Infections: Strengths and Limitations. Immune Netw. *21*, e12. https://doi.org/10.4110/in.2021.21.e12.
107. Brocato, R.L., Principe, L.M., Kim, R.K., Zeng, X., Williams, J.A., Liu, Y., Li, R., Smith, J.M., Golden, J.W., Gangemi, D., et al. (2020). Disruption of Adaptive Immunity Enhances Disease in SARS-CoV-2-Infected Syrian Hamsters. J. Virol. *94*, e01683-20. https://doi.org/10.1128/JVI.01683-20.
108. Osterrieder, N., Bertzbach, L.D., Dietert, K., Abdelgawad, A., Vladimirova, D., Kunec, D., Hoffmann, D., Beer, M., Gruber, A.D., and Trimpert, J. (2020). Age-Dependent Progression of SARS-CoV-2 Infection in Syrian Hamsters. Viruses *12*, 779. https://doi.org/10.3390/v12070779.
109. Mendoza, E.J., Manguiat, K., Wood, H., and Drebot, M. (2020). Two Detailed Plaque Assay Protocols for the Quantification of Infectious SARS-CoV-2. Curr. Protoc. Microbiol. *57*, ecpmc105. https://doi.org/10.1002/cpmc.105.
110. Wölfel, R., Corman, V.M., Guggemos, W., Seilmaier, M., Zange, S., Muller, M.A., Niemeyer, D., Jones, T.C., Vollmar, P., Rothe, C., et al. (2020). Virological assessment of hospitalized patients with COVID-2019. Nature *581*, 465–469. https://doi.org/10.1038/s41586-020-2196-x.
111. Cantor, J.R., Abu-Remaileh, M., Kanarek, N., Freinkman, E., Gao, X., Louissaint, A., Jr., Lewis, C.A., and Sabatini, D.M. (2017). Physiologic Medium Rewires Cellular Metabolism and Reveals Uric Acid as an Endogenous Inhibitor of UMP Synthase. Cell *169*, 258–272.e17. https://doi.org/10.1016/j.cell.2017.03.023.
112. Li, B., Tang, J., Yang, Q., Li, S., Cui, X., Li, Y., Chen, Y., Xue, W., Li, X., and Zhu, F. (2017). NOREVA: normalization and evaluation of MS-based metabolomics data. Nucleic Acids Res. *45*, W162–W170. https://doi.org/10.1093/nar/gkx449.
113. Ritchie, M.E., Phipson, B., Wu, D., Hu, Y., Law, C.W., Shi, W., and Smyth, G.K. (2015). limma powers differential expression analyses for RNA-sequencing and microarray studies. Nucleic Acids Res. *43*, e47. https://doi.org/10.1093/nar/gkv007.

STAR★METHODS

KEY RESOURCES TABLE

REAGENT or RESOURCE	SOURCE	IDENTIFIER
Antibodies		
Anti SARS-CoV-2 spike protein antibody	Novus Biologicals	NBP3-11940
Anti SARS-CoV-2 nucleocapsid protein antibody	Novus Biologicals	NB100-56576
Anti-IDO	Cell Signaling Technology	86630S
Anti Arg 1	Cell Signaling Technology	93668S
Anti-β-actin	Cell Signaling Technology	4976S
Anti-rabbit IgG1 HRP-linked	Cell Signaling Technology	7074S
Bacterial and virus strains		
SARS-CoV-2 isolate USA-WI1/2020	BEI	NR-52384
SARS-CoV-2, Isolate hCoV-19/USA/PHC658/2021 (Lineage B.1.617.2; Delta Variant)	BEI	NR-55611
SARS-CoV-2, Isolate hCoV-19/USA/GA-EHC-2811C/ 2021 (Lineage B.1.1.529; Omicron Variant)	BEI	NR-56481
Chemicals, peptides, and recombinant proteins		
Viral Transport Medium	Innovative Research, Inc	IGVTM500ML-35403
IDO1 inhibitor (Indoximod)	MedChemExpress	HY-16724
Recombinant human IL-10	PeproTech	200–10
Recombinant human IFN-g	PeproTech	300–02
Recombinant human IL-4	PeproTech	200–04
Hematoxylin	Leica Biosystems	3801560
Eosin	Ricca Chemical Company	2850–16
Picro Sirius Red solution	Hello Bio	HB9475
Eagle's Minimum Essential Medium	ATCC	30–2003
L-glutamine	Thermo Scientific	25030081
Penicillin-Streptomycin (10,000 U/mL)	Thermo Scientific	15140122
Avidin-Biotinylated HRP, 3,3′-diaminobenzidine (DAB)	Vector Laboratories	PK-6100
Critical commercial assays		
RNeasy Mini Kit	Qiagen	74104
QIAamp Viral RNA Mini Kit	Qiagen	52904
iScript cDNA Synthesis Kit	Bio-Rad laboratories	1708890
HRP-conjugated secondary antibody	Jackson ImmunoResearch	123-055-021
Chemiluminescent substrate	Thermo Scientific	34579
Deposited data		
Hamsters Lung Metabolomics	Metabolomics Core Facility University of Iowa	https://doi.org/10.6084/m9.figshare.25180466
Experimental models: cell lines		
LVG Golden Syrian Hamster	Charles River Laboratories	Crl:LVG(SYR)
Calu-3	ATCC	HTB-55
Vero-E6	ATCC	CRL-1586
Experimental models: organisms/strains		
Golden Syrian hamsters	Charles River Laboratories	Crl:LVG(SYR)

(*Continued on next page*)

Continued

REAGENT or RESOURCE	SOURCE	IDENTIFIER
Oligonucleotides		
Forward primer for SARS-CoV-2 E gene 5′–ACAGGTACGTTAATAGTTAATAGCGT–3′	Integrated DNA Technologies	
Reverse primer for SARS-CoV-2 E gene 5′–ATATTGCAGCAGTACGCACACA–3′	Integrated DNA Technologies	
Probe for SARS-CoV-2 E gene 5′– FAM–ACACTAGCCATCCTTACTGCGCTTCG-BHQ1–3′	Integrated DNA Technologies	
Forward primer for SARS-CoV-2 N gene 5′– CGATCTCTTGTAGATCTGTTCTC–3′	Integrated DNA Technologies	
Reverse primer for SARS-CoV-2 N gene 5′–TCTGGTTACTGCCAGTTGAATCTG–3′	Integrated DNA Technologies	
Probe for SARS-CoV-2 N gene 5′– FAM– ACCCCGCATTACGTTTGGTGGACC-BHQ1–3′	Integrated DNA Technologies	
Human RT-qPCR primers		
TNF-α F: 5′-CTCTTCTGCCTGCTGCACTTTG-3′ R: 5′-ATGGGCTACAGGCTTGTCACTC-3′	Integrated DNA Technologies	
IL-6 F: 5′-AGACAGCCACTCACCTCTTCAG-3′ R: 5′-TTCTGCCAGTGCCTCTTTGCTG-3′	Integrated DNA Technologies	
IL-10 F: 5′-GACTTTAAGGGTTACCTGGGTTG-3′ R: 5′-TCACATGCGCCTTGATGTCTG-3′	Integrated DNA Technologies	
ISG15 F: 5′-CTCTGAGCATCCTGGTGAGGAA-3′ R: 5′-AAGGTCAGCCAGAACAGGTCGT-3′	Integrated DNA Technologies	
CXCL10 F: 5′-GGTGAGAAGAGATGTCTGAATCC-3′ R: 5′-GTCCATCCTTGGAAGCACTGCA-3′	Integrated DNA Technologies	
ARG1 F: 5′-TCATCTGGGTGGATGCTCACAC-3′ R: 5′-GAGAATCCTGGCACATCGGGAA-3′	Integrated DNA Technologies	
iNOS F: 5′-GCTCTACACCTCCAATGTGACC-3′ R: 5′-CTGCCGAGATTTGAGCCTCATG-3′	Integrated DNA Technologies	
IDO-1 F: 5′-GCCAGCTTCGAGAAAGAGTTG-3′ IDO-1 R: 5′-ATCCCAGAACTAGACGTGCAA-3′	Integrated DNA Technologies	
GAPDH F: 5′-GTCTCCTCTGACTTCAACAGCG-3′ R: 5′-ACCACCCTGTTGCTGTAGCCAA-3′	Integrated DNA Technologies	
Hamsters RT-qPCR primers		
TNF F: 5′-TGAGCCATCGTGCCAATG-3′ R: 5′-AGCCCGTCTGCTGGTATCAC-3′	Integrated DNA Technologies	
IL-6 F: 5′-GGACAATGACTATGTGTTGTTAGAA-3′ R: 5′-AGGCAAATTTCCCAATTGTATCCAG-3′	Integrated DNA Technologies	
IFN-γ F: 5′-TGTTGCTCTGCCTCACTCAGG-3′ R: 5′-AAGACGAGGTCCCCTCCATTC-3′	Integrated DNA Technologies	
IL-4 F: 5′-CCACGGAGAAAGACCTCATCTG-3′ R: 5′-GGGTCACCTCATGTTGGAAATAAA-3′	Integrated DNA Technologies	
ISG15 F: 5′-AAAGCCTACAGCCATGACCT-3′ R: 5′-TTAGTCAGGGGCACCAGGAA-3′	Integrated DNA Technologies	
CXCL10 F: 5′-GCCATTCATCCACAGTTGACA-3′ R: 5′-CATGGTGCTGACAGTGGAGTCT-3′	Integrated DNA Technologies	
CCL5 F: 5′-ACTGCCTCGTGTTCACATCA-3′ R: 5′-CCTTCGGGTGACAAAAACGA-3′	Integrated DNA Technologies	

(*Continued on next page*)

Continued

REAGENT or RESOURCE	SOURCE	IDENTIFIER
ARG1 F: 5′-ACCTATGTGTCATTTGGGTGGA-3′ R: 5′-GCAGATATGCAGGGAGTCACC-3′	Integrated DNA Technologies	
iNOS F: 5′-CGACGGCACCATCAGAGG-3′ R: 5′-AGGATCAGAGGCAGCACATC-3′	Integrated DNA Technologies	
IDO-1 F: 5′-TCCCACTGAAGGTTCTAGGAAGA-3′ R: 5′-TACTAGCAATGCGGGTCCAG-3′	Integrated DNA Technologies	
GAPDH F: 5′-GCATGGCCTTCCGTGTCC-3′ R: 5′-TGTCATCATACTTGGCAGGTTTCT-3′	Integrated DNA Technologies	
GAPDH	Integrated DNA Technologies	
Software and algorithms		
limma v3.50.0	limma_3.58.1.tar.gz	https://bioinf.wehi.edu.au/limma/
ComplexHeatmap v2.2.0	ComplexHeatmap_2.18.0.tar.gz	https://github.com/jokergoo/ComplexHeatmap https://jokergoo.github.io/ComplexHeatmap-reference/book/
PCAtools v2.6.0	https://github.com/kevinblighe/PCAtools	
ImageJ	NIH	https://imagej.nih.gov/ij/download.html
GraphPad Prism v9.0	GraphPad	https://www.graphpad.com/
Biorender	Biorender	https://www.biorender.com

RESOURCE AVAILABILITY

Lead contact

Further information and requests for resources and reagents should be directed to and will be fulfilled by the Lead Contact, Siddappa N. Byrareddy (sid.byrareddy@unmc.edu).

Materials availability

This study did not generate new unique reagents.

Data and code availability

Metabolomics data have been deposited in the figshare: https://doi.org/10.6084/m9.figshare.25180466.

EXPERIMENTAL MODEL AND STUDY PARTICIPANT DETAILS

Cell lines

Vero-E6 and Calu-3 (ATCC HTB-55; mycoplasma negative) cells were grown at 37°C and 5% CO_2 in Eagle's Minimum Essential Medium (ATCC 30–2003) containing 10% FBS, 2 mM L-glutamine, 100 units/ml penicillin, 100 units/ml streptomycin.

Viral stocks

SARS-Related Coronavirus 2, Isolate USA-WI1/2020 (# NR-52384), SARS-Related Coronavirus 2, Isolate hCoV-19/USA/PHC658/2021 (Lineage B.1.617.2; Delta Variant; # NR-55611) and SARS-Related Coronavirus 2, Isolate hCoV-19/USA/GA-EHC-2811C/2021 (Lineage B.1.1.529; Omicron Variant; # NR-56481) were obtained through BEI Resources. All viruses were grown and amplified in Calu-3 cells. Vero-E6 cells were used to titer the virus using the plaque assay.[109] The viral stocks used in cell culture and animal studies were generated in passages 1–2 of the initial stock obtained from BEI Resources.

Study approval

All infectious work with SARS-CoV-2 was performed in biosafety level 3 laboratory facilities at Durham Research Center, the University of Nebraska Medical Center (UNMC) under the supervision of trained veterinary staff. All the animals infected by SARS-CoV-2 were handled in a biosafety level 3 animal facilities in accordance with the Guide for the Care and Use of Laboratory Animals of the National Institutes of Health and the Guidelines to promote the wellbeing of animals used for Scientific purposes. The protocols were approved by the Institutional Animal Care and Use Committee at UNMC (protocol # 21-019-06-FC).

METHOD DETAILS

Hamster study

Thirty-two male Syrian golden hamsters (8–10 weeks of age) were used in this study, purchased from Charles River Laboratories. All animals were randomized and assigned to three groups. 4 hamsters were used as uninfected controls. Sixteen hamsters were infected with Delta variants (10 necropsied at 4 DPI and 6 necropsied at 10 DPI) and 12 hamsters were infected with Omicron variants (6 necropsied at 4 DPI and 6 necropsied at 10 DPI), respectively. All animals were given a code that is known only to the veterinarians, and all the animal works were conducted at the comparative medicine (CM) department of UNMC that including virus inoculation, daily body weight and temperature monitoring, and necropsy at day 4 and day 10 post-infection. On necropsy days, the CM personnel harvested the tissues and body fluids and handed over to our lab personnel for downstream analysis.

Hamsters infection

Four hamsters were used as uninfected/naive controls. On day 0, hamsters were infected with SARS-CoV-2 (1.6×10^4 PFU/animal), the Delta (B.1.617.2; 16 animals), and the Omicron (B.1.1.529; 12 animals) variants via intranasal route. Body weight was recorded daily (0–10 days) to evaluate weight changes. In a viral Transport medium, oral swabs were collected every other day (days 0, 2, 4, 6, 8, and 10). On day 4 post-infection (DPI), 10 hamsters from the Delta-infected group and six from the Omicron-infected group were euthanized. On 10 DPI, six animals from Delta- and omicron-infected groups were euthanized for collection of lungs, trachea, nasal turbinates, and brain tissues. Food and water were available *ad libitum*, and hamsters were euthanized humanely to improve animal welfare and minimize suffering.

Cell culture

Both Vero-E6 and Calu-3 (ATCC HTB-55; mycoplasma negative) cells were grown at 37°C and 5% CO_2 in Eagle's Minimum Essential Medium (ATCC 30–2003) containing 10% FBS, 2 mM L-glutamine, 100 units/ml penicillin, 100 units/ml streptomycin.

SARS-CoV-2 viral stocks

SARS-Related Coronavirus 2, Isolate USA-WI1/2020 (# NR-52384), SARS-Related Coronavirus 2, Isolate hCoV-19/USA/PHC658/2021 (Lineage B.1.617.2; Delta Variant; # NR-55611) and SARS-Related Coronavirus 2, Isolate hCoV-19/USA/GA-EHC-2811C/2021 (Lineage B.1.1.529; Omicron Variant; # NR-56481) were obtained through BEI Resources. All viruses were grown and amplified in Calu-3 cells. Vero-E6 cells were used to titer the virus using the plaque assay.[109] The viral stocks used in cell culture and animal studies were generated in passages 1–2 of the initial stock obtained from BEI Resources.

RNA isolation and RT-qPCR

RNA from oral swab samples was isolated using the QIAamp Viral RNA Mini Kit (QIAGEN) according to manufacturer specifications. Lungs, trachea, nasal turbinates, and brain tissues were homogenized in RLT tissue lysis buffer using Tissue Lyser (Qiagen), and RNA was extracted using the RNeasy Mini Kit (QIAGEN) according to manufacturer specifications. One-step RT-qPCR was performed to quantitate viral genomic (E gene) and subgenomic (N subgene) from oral swabs and tissues using specific primer-probes[110] and QuantStudio3 real-time PCR system (Applied Biosystems) per manufacturer's specifications. SARS-CoV-2 E and 2 N subgene-specific primers are described above. Viral RNA copies in oral swabs and tissues were quantitated using dilutions of SARS-CoV-2 standards with a known concentration of RNA copies. Differential gene expression of cytokines/chemokines/ISGs and metabolic enzymes was analyzed by RT-qPCR using SyBR green per the manufacturer's guidelines in the QuantStudio3 real-time PCR system (Applied Biosystems). Briefly, RNA extracted from lungs and brain tissues was reverse transcribed into cDNA using iScript cDNA synthesis Kit (Bio-Rad laboratories). PCR was conducted in a 10 μL reaction volume containing a 20 ng cDNA template and 3 μM hamster gene-specific primers.

Histology (H & E) and immunohistochemistry (IHC)

Lungs and brain tissues from naive, Delta- and Omicron-infected, and PBS-perfused hamsters were fixed in 10% neutral phosphate-buffered formalin for a minimum of 3 days. Tissues were placed in cassettes and processed in STP 120 (Thermo Scientific) tissue processor using a graded series of ethanol, xylene, and paraffin wax. Embedded tissues were sectioned at 5 μm and processed for histopathology by hematoxylin and eosin (H&E) staining using a standard hematoxylin and eosin procedure and photographed. H & E-stained slides were evaluated blindly by a board-certified pathologist, and the score was 0: no pathology, 1: minimal, 2: mild to moderate, and 3: severe.

For IHC staining, tissue sections were deparaffinized, and the antigen retrieval process was performed using a decloaking chamber (Biomedical care). Then, tissue sections were blocked by blocking buffer and incubated overnight with anti-nucleocapsid (NB100-56576) or anti-spike (NBP3-11940; Novus Biologicals) primary antibodies at 4°C. Next day, and tissue sections were washed and incubated with biotinylated secondary antibody (Vector IHC kit, Newark, CA, USA) at room temperature for 1 h and washed. Tissue slides were incubated with Avidin-Biotinylated HRP (Vectastain, Vector Laboratories) for 30 min and developed with peroxidase substrate (3,3′-diaminobenzidine (DAB), Vector kit). Dehydrated tissues were mounted with coverslips, and images were captured under a microscope ((BioTek, Santa Clara, CA) using Gen5 3.05 software.

LC-MS metabolomic profile of hamster lung tissues

The targeted metabolomic profile was performed at the Metabolomics Core Facility at the University of Iowa, Carver College of Medicine, Iowa. Tissue samples were lyophilized, transferred to ceramic bead tubes, and homogenized in extraction solvent (18-fold (w/v)). Then, samples were rotated at −20°C for 1 h and centrifuged at 21,000 *g* for 10 m. The supernatants (400 μL) were transferred to 1.5 mL Eppendorf tubes, vortexed, and dried using a speed vac apparatus. Dried extracts were reconstituted in 20 μL acetonitrile/water (1:1 v/v), vortexed, and rotated on a rotator at −20°C overnight. The reconstituted samples were centrifuged, and the supernatant was transferred to LC-MS autosampler vials for analysis. LC-MS data were acquired on a Thermo Q Exactive hybrid quadrupole Orbitrap mass spectrometer with a Vanquish Flex UHPLC system or Vanquish Horizon UHPLC system. A Millipore SeQuant ZIC-pHILIC (2.1 × 150 mm, 5 μm particle size) with a ZIC-pHILIC guard column (20 × 2.1 mm) was used as an LC column with an injection volume of 2 μL. The method was run at a flow rate of 0.150 mL/min using solvent A (20 mM ammonium carbonate [$(NH_4)_2CO_3$] and 0.1% Ammonium Hydroxide (v/v) [NH_4OH] with pH ~9.1) and solvent B (acetonitrile). The gradient starts at 80% B and decreases to 20% B over 20 min; returning to 80% B in 0.5 min; and held there for 7 min. The mass spectrometer was operated in full-scan, polarity-switching mode from 1 to 20 min, with the spray voltage set to 3.0 kV, the heated capillary held at 275°C, and the HESI probe held at 350°C. The sheath gas flow was set to 40 units, the auxiliary gas flow was set to 15 units, and the sweep gas flow was set to 1 unit. MS data acquisition was performed in a range of m/z 70–1,000, with the resolution set at 70,000, the AGC target at 1×10^6, and the maximum injection time at 200 ms.[111] Acquired LC-MS data were processed by Thermo Scientific TraceFinder 4.1 software, and metabolites were identified based on the University of Iowa Metabolomics Core facility standard-confirmed, in-house library. NOREVA was used for signal drift correction[112] and data were normalized to the sum of all the measured metabolite ions in that sample.

Calu-3 cells infection with SARS-CoV-2 variants

Calu-3 cells (2×10^5/well) were infected with either 0.1 or 0.5 MOI of SARS-CoV-2 variants (WI, Delta and Omicron) and incubated for 24 h. Cells were washed with PBS and lysed with RLT buffer corresponding to 24 h time point. For 48 h and 72 h time points, infected cells were replaced with fresh EMEM medium and continued incubation for 24 h (corresponds to 48 h) and 48 h (corresponds to 72 h). RNA was extracted using the RNeasy Mini Kit (QIAGEN) according to manufacturer specifications. One-step RT-qPCR was performed to quantitate viral genomic (E gene) and subgenomic (N subgene) RNA from oral swabs and tissues using specific primer probes described above.

In another experiment, Calu-3 cells were pretreated in the absence or presence of indoximod (0.1–75 μM)/IL-10 (5–25 ng/mL)/IFN-g (10–20 ng/mL) for 1 h in 24 well cell culture plates. Then, cells were infected with SARS-CoV-2 (Delta variant) for 16 h. Cells were washed with PBS and replaced with fresh EMEM medium without or with respective concentrations of indoximod/IL-10/IFN-g and continued incubation for 24 h. Then, RNA was isolated and quantitated for viral RNA E gene and N subgene. RNA was reverse transcribed to cDNA using iScript cDNA synthesis kit and quantitated for SARS-CoV-2-induced gene expression profile of cytokines/chemokines/ISGs and metabolic enzymes using human gene-specific primers.

Western blotting

Calu-3 cells (1×10^6/well) were infected with SARS-CoV-2 as described earlier. Whole-cell lysates were prepared by the addition of lysis buffer (Cell Signaling Technology) and subsequent incubation at 4°C. Cell lysates were separated by electrophoresis in a denaturing SDS/PAGE gel under reducing condition and transferred to a PVDF membrane at constant voltage (100 V). Blots were blocked with 5% fat-free milk in TBST and incubated overnight in relevant primary antibodies at 4°C. Membranes were washed four to five times with TBST and incubated with appropriate HRP-conjugated secondary antibody (Jackson ImmunoResearch). Blots were developed using a Chemiluminescent substrate (SuperSignal West Atto Ultimate Sensitivity; Thermo Scientific).

QUANTIFICATION AND STATISTICAL ANALYSIS

Statistical significance (p values < 0.05) was assessed in hamster experiments using two-way ANOVA with Sidak's multiple comparisons test. One-way ANOVA with multiple comparisons test was performed to assess statistical significance (p values < 0.05) using GraphPad PRISM 9.0 (GraphPad Software). Principal component analysis (PCA) was performed using R package PCAtools v2.6.0 (https://github.com/kevinblighe/PCAtools), and differential regulation analysis was executed using R package limma v3.50.0.[113] Both PCA and differential regulation analysis was done using log2 transformed metabolomics data. A threshold of adj p < 0.1 was considered to define a significant abundance of metabolites in any pairwise comparison.